POLITECNICO DI MILANO

Facoltà di Ingegneria Industriale
e dell'informazione

Corso di Laurea Magistrale in
Ingegneria Energetica

Experimental analysis of air-water two-phase flow in vertical large pipes and development of drift-flux models

Relatore: Prof. Fabio INZOLI

Tesi di Laurea Magistrale di:
Ruben POMPILIO   Matr. 783006

Anno Accademico 2012-2013

Ringraziamenti

A Mirella e Dino

Contents

Abstract

In this thesis is provided a revision of the mechanisms governing the two-phase flow, particularly in large diameter vertical pipes. Is reported the equations that govern the physics and the measurement methods used in order to better understand the problem of coexistence of two phases of different nature. We are focused on the drift-flux model as a simple, compact solution for the calculation of the void fraction. Two different models are developed: one, a comprehensive drift-flux model, applicable to a variety of facility configurations and operating conditions; the other specifically developed for the facility in the laboratory of the Politecnico di Milano. This laboratory is also used to collect data and test the optical probes.

Keywords: two-phase flow, drift-flux models, large pipes, experimental facility

In questa tesi è riportata una revisione dei meccanismi che regolano il flusso bifase, in particolare in condotte di grosso diametro. Sono riportate le equazioni fenomenologiche che governano la fisica e i metodi di misurazione utilizzati al fine di comprendere meglio il problema della coesistenza di due fasi di diversa natura. Si pone attenzione sulla modellistica drift-flux come una soluzione semplice e compatta per il calcolo della frazione di vuoto. Due modelli differenti sono stati sviluppati e riportati: il primo riguarda un modello generalizzato per condotte verticali (estendibile in parte a condotte con differente inclinazione) di tipo drift-flux applicabile a una varietà di configurazioni impiantistiche e condizioni operative; il secondo, specificamente sviluppato per l'impianto presente nel laboratorio del Politecnico di Milano al fine di predire la frazione di vuoto nell'impianto. Il laboratorio è stato progettato e realizzato per raccogliere dati, necessari allo sviluppo del modello, tramite parametri globali e sonde ottiche.

Parole chiave: Flussi bifase, modelli drift-flux, condotte di grosso diametro, impianti sperimentali

Abstract esteso

Ai giorni nostri è sempre più importante la conoscenza approfondita dei sistemi multifase, questo perché sono sempre più presenti nella quotidianità industriale. Questi sistemi, infatti, riguardano le più svariate applicazioni: dai reattori nucleari ai motori a vapore, dagli scambiatori di calore alle colonne di distillazione chimica, dal trasporto degli idrocarburi nelle condotte ai sistemi biologici di trasporto dei fluidi corporei. Una problematica sempre più sentita riguarda l'impiego del calcolatore come mezzo per la previsione del comportamento dei sistemi multifase. Infatti, per poter simulare il comportamento di un grande sistema sarebbe necessario il calcolo di estesi sistemi di equazioni, con impiego di grosse risorse computazionali non senza l'introduzione di errori di tipo modellistico e di approssimazione.

Un sistema bifase è composto da due o più fluidi legati più o meno intimamente tra loro; vi è la presenza di una discontinuità rappresentata dall'interfaccia tra i due fluidi ove avviene lo scambio di massa, di quantità di moto e di energia. Questa interfaccia è la principale causa della complessità del sistema bifase e da qui derivano tutte le problematiche relative alla simulazione del comportamento della stessa con i moderni codici di calcolo. Mentre il flusso monofase può essere categorizzato in base al tipo di struttura: laminare o turbolento; il flusso bifase è categorizzato in base ai regimi di flusso. Vi è la possibilità di affrontare il problema fisico del bifase con un approccio basato sulle equazioni per il monofase applicate singolarmente ad ogni fluido presente, ma questo comporterebbe difficoltà computazionali enormi per la maggior parte dei sistemi industriali. Bisogna ricorrere ad un approccio globale che permetta di ricavare le informazioni principali, senza entrare troppo nello specifico.

Per caratterizzare i flussi bifase è necessaria l'introduzione di una serie di parametri: la frazione di vuoto, che rappresenta il rapporto tra il volume della fase dispersa (o gas) e il volume totale; le velocità superficiali e le velocità di fase, che sono legate tra di loro tramite la frazione di vuoto e rappresentano la portata volumetrica per unità di area di passaggio; il diametro idraulico, usato come principale grandezza caratteristica per definire la geometria del sistema a cui sono legate le strutture fluidodinamiche che si andranno a sviluppare all'interno del sistema; le proprietà fisiche dei fluidi, in

particolare la viscosità cinematica e la tensione superficiale, anch'esse responsabili della dinamica all'interno delle condotte; temperatura e pressione, che hanno diretto effetto sulle densità; infine, il diametro delle bolle sviluppate, rappresentato dal diametro medio di sauter, che influisce direttamente sui coefficienti di scambio di massa tra i due fluidi.

La problematica relativa alle equazioni che governano il sistema bifase può essere brevemente ricondotta al problema della formulazione istantanea delle equazioni stesse; infatti le difficoltà matematiche introdotte da una formulazione di questo tipo sono legate: alla deformabilità dell'interfaccia tra i fluidi e alla presenza della turbolenza. Problemi già di per se molto grandi per un flusso monofase. Per ovviare a questa formulazione complessa e poco performante è richiesta l'introduzione di metodi di mediazione delle equazioni; quello più usato è la media euleriana. L'applicazione di questa "media" permette di correlare le condizioni al contorno del problema con i dati ricavati sperimentalmente e ottenere delle equazioni in grado di fare delle previsioni degli eventi macroscopici.

A tal proposito sono presi in considerazione di modelli drift-flux che sono complementari ai modelli two-fluids. Il vantaggio dei primi risiede nel fatto che semplifica il problema considerando il sistema bifase come un unica miscela, in cui gli effetti di una fase rispetto all'altra sono tenuti in considerazione tramite un parametro chiamato *velocità di drift*. Ovviamente questa semplificazione la si paga con una minore precisione sulla previsione. L'impiego dei modelli drift-flux ha trovato largo impiego nelle applicazioni industriali, proprio per la sua compattezza e semplicità. Per derivare la formulazione ottenuta da Zuber negli anni '60 è necessario partire dalle equazioni in forma monodimensionale, che a loro volta derivano dalle equazioni della meccanica dei fluidi; successivamente si applica la media integrale sull'area e la media pesata sulla frazione di vuoto, ottenendo così quattro equazioni: la continuità per la miscela e per una delle due fasi (la fase gas), l'equazione del momento della quantità di moto e l'equazione dell'energia. In tutte queste equazioni sono presenti termini che tengono in considerazioni gli effetti dell'interazione tra i due fluidi. Questi coefficienti devono essere modellizzati per avere la "chiusura" delle equazioni. Partendo dalla definizione di velocità di drift, di velocità di fase e con l'ausilio della definizione dei parametri del modello drift-flux si arriva alla sua definizione completa. Si tratta di una equazione algebrica lineare in cui la velocità della fase gas è in funzione del flusso volumetrico della miscela tramite i due coefficienti

del modello: il parametro di distribuzione, che rende conto della distribuzione della fase gas lungo la direzione radiale; la velocità di drift che tiene da conto l'interazione tra i fluidi. Questi parametri possono essere ricavati sperimentalmente per poter creare un modello adatto ad un particolare impianto oppure calcolati teoricamente tramite considerazioni fluidodinamiche sui flussi nelle condotte.

L'aspetto sperimentale non può essere trascurato, in particolare per i sistemi bifase, la cui natura complessa spesso esula dalle nostre possibilità informatiche. E' necessario conoscere, quindi, i principali metodi di misura proposti nella letteratura per avere la possibilità di ricavare più informazioni possibili da un impianto reale. Le tecniche di misura si suddividono in quattro gradi categorie: l'osservazione visuale, che è la più semplice e permette di ottenere le prime informazioni sulla struttura del flusso; l'osservazione di parametri globali, come la frazione di vuoto in funzione della perdita di carico; le grandezze variabili nel tempo, come la fluttuazione della frazione di vuoto, della pressione e della temperatura, il numero di bolle e il loro diametro; le tecniche di misura avanzate, che prevedono l'impiego di sofisticati strumenti di misura come i densitometri a raggi gamma e strumenti che sfruttano l'effetto Doppler. L'analisi a posteriori dei dati ricavati permette di evidenziare gli aspetti peculiari del flusso bifase e di categorizzare i vari regimi. Gli strumenti più usati sono l'analisi statistica dei segnali della frazione di vuoto nel tempo affiancate da reti neurali in grado di riconoscere la tipologia dei dati e creare un sistema di categorie.

La grande differenza tra flussi monofase e bifase si riscontra nella variabilità delle strutture fluidodinamiche in funzione della dimensione fisica del condotto in cui scorrono i fluidi. La distinzione tra tubi piccoli e grossi avviene tramite l'impiego del diametro idraulico opportunamente adimensionalizzato. I tre principali effetti che si riscontrano nelle grosse condotte rispetto alle piccole sono: diminuzione del numero delle bolle di Taylor, che influiscono sulla distribuzione radiale della frazione di vuoto; riduzione dell'influenza delle pareti del tubo sul flusso; presenza di forte ricircolazione soprattutto in sistemi controcorrente anche a basse velocità del liquido. I regimi di flusso che si instaureranno saranno funzione degli effetti sopra elencati.

I regimi di flusso che si possono instaurare nelle condotte verticali (e ormai accettati da tutto il mondo scientifico) sono principalmente quattro e sono ordinati in base alla crescente portata volumetrica di gas: flusso a bolle, caratterizzato dalla presenza di

piccole bolle che si muovono in maniera ordinata; flusso a grosse bolle; flusso a frotti, che è il più caotico, in cui vi è forte presenza di turbolenza e di ricircolazioni; flusso anulare, in cui si ha un film di liquido a parete e un flusso di gas al centro. Il modo in cui viene iniettata la fase gas nel sistema ha effetti importanti sia sulla lunghezza necessaria affinché si raggiunga un flusso pienamente sviluppato, sia sulla previsione della frazione di vuoto, soprattutto a basse portate di fluido.

Convenzionalmente, i dati sperimentali sono raccolti in *mappe di flusso* che permettono di riconoscere i vari regimi di flusso. Per fare ciò è necessario sviluppare dei criteri di transizione che permettano di valutare teoricamente i confini tra i regimi stessi. Ovviamente, questi criteri sono delle correlazioni algebriche che sono influenzate dalle grandezze fisiche del sistema e dalle proprietà fisiche dei fluidi.

L'impianto sperimentale realizzato presso i laboratori del Politecnico di Milano serve proprio allo scopo di condurre esperimenti per ampliare la conoscenza del comportamento dei flussi bifase aria-acqua in condotte verticali di grosso diametro. Le tecniche di misura utilizzate per ricavare i dati sulla frazione di vuoto sono: l'osservazione diretta, la valutazione della stessa tramite parametri globali e l'impiego di sonde ottiche. Queste ultime permettono di ricavare molte informazioni utili sul flusso in esame tra cui: numero di bolle, dimensione, velocità e frazione di vuoto. La campagna sperimentale è stata condotta su una mappa di flusso in 13 portate di gas e 10 di liquido, per un totale di 130 punti di funzionamento, adatti per ricavare dati di frazione di vuoto compresi tra 0 e 0.3.

In questa tesi vengono proposti due modelli: uno che raccoglie diversi modelli presi dalla letteratura per poterne ampliare il campo di funzionamento e l'affidabilità predittiva degli impianti equicorrente verso l'alto; l'altro realizzato specificatamente per l'impianto del Politecnico al fine di predire la frazione di vuoto.

Per il primo modello si è analizzata la letteratura e si sono raccolti i modelli necessari al calcolo della frazione di vuoto sia in tubi piccoli che i quelli a grosso diametro. Si sono introdotti dei metodi interpolatori di natura esponenziale al fine di coprire l'intero campo di possibili condizioni operative industriali sia per i regimi di flusso, sia per di diametri. La validazione del modello è stata fatta tramite il confronto con 10 database trovati in letteratura per i tubi grossi e 9 per quelli di piccolo diametro. Sono state

testate anche altre configurazioni come quella orizzontale, equicorrente verso il basso e controcorrente, ottenendo risultati soddisfacenti.

L'ultimo modello non ha pretesa di validità generale, ma permette di predire la frazione di vuoto nell'impianto del Politecnico di Milano. Questo modello potrà essere implementato, in futuro, in codici più complessi per il calcolo fluidodinamico. Il modello è stato testato con dati provenienti da impianti con colonne a gorgogliamento, poiché in letteratura è assai difficile reperire dati di impianti simili al nostro, poiché si tratta di impianti pilota.

Il calcolo della frazione di vuoto e della grandezze ad essa correlate è di fondamentale utilità per i sistemi multifase, come il trasporto del greggio. I modelli drift-flux sono importanti per il calcolo indiretto delle perdite di carico nelle condotte.

Chapter 1

INTRODUCTION

Nowadays there is a general interest for even more accurate predictions of multiphase flows in engineering systems. In particular, during the design of these systems, several issues may appear during the scale up of pilot plants. These issues can be faced if proper prediction of the physics governing the multiphase flow is accounted for during the design of the system. This means a shift of design methods from the ones exclusively based on static experimental correlations to the ones based on mathematical models that can predict dynamical behaviors of systems. A new generation of multiphase codes and models will allow to design and test a lot of physical systems in a less expansive manner, without the construction of expensive full-scale models. This will reduce the expense and time associated with the real construction scale.

The subject of two (or multiphase) flow is very important in a wide variety of engineering systems. Some relevant engineering systems are for instance:

- BWR & PWR nuclear reactors;

- Steam Rankine cycle;

- Internal combustion engines;

- Heat exchangers and storage;

- Chemical reactors;

- Pipeline transport of gas and oil mixtures;

- Cavitation;

- Cardiovascular system.

1.1   Characteristics of multiphase flow

The understanding of the thermo-fluid dynamics of two-phase flow and the predictive capability have still not attained the level available for single-phase flow analyses. Because of this, the tendency has been to analyze the problems of a particular system and develop specific models and correlations of limited generality and applicability. The ability to predict the performance of systems depends on the availability of experimental data and of mathematical models that can be used to describe the physical processes with a required degree of accuracy.

The complex nature of two-phase flow originates from the existence of multiple, deformable and moving interfaces that casues a significant discontinuities of fluid properties and complicated flow field near the interface. Single-phase flow can be classified according to the structure of flow into: laminar, transitional and turbulent flow. In contrast, two-phase flow can be classified according to the structure of interface into several major groups, which can be called flow regimes, or flow patterns such as: separated flow, mixed flow and dispersed flow. It can be expected (similar to single-phase flow) that many of two-phase flow systems should exhibit physical similarities when the flow regimes are the same.

For most engineering problems the local formulation, based on the single-phase flow formulation with explicit moving interfaces, is not a practical approach. This leads to the need of a macroscopic formulation based on proper averaging which gives a two-phase flow continuum formulation by eliminating the interfacial discontinuities.

Each approach to the multi-phase fluid dynamics is multi-scale and the degree of complexity depend on how we go deep inside the physical aspect. In the macro-scale are accounted the transport of mass, momentum and energy. In the meso-scale are accounted the turbulence effects for momentum and energy, the interfacial exchanges for mass. In the micro-scale are accounted the effects of wall nucleation and bubble coalescence and break-up.

1.2 Two-phase flow parameters

All of the subsequent parameters come together to define the fluid dynamics of multi-phase flow. For convenience, the term of *dispersed phase* will be used for the bubbles, droplets or particles, while *continuous phase* will be used for the carrier fluid.

1.2.1 Void fraction

In two-phase flow analysis, the *void fraction* and the *interfacial area concentration* represents the two fundamental geometrical parameters and they are closely related to two-phase flow regimes. The concept of the two-phase flow regimes is often difficult to quantify mathematically, this may indicate that the modeling of the changes of the interfacial area concentration directly by a transport equation is a better approach than the conventional method using the regime-dependent constitutive relations.

The volume fraction of the dispersed phase, named *void fraction*, is defined as:

$$\alpha_g = \lim_{V \to V^0} \frac{V_g}{V} \tag{1.1}$$

where V_g is the volume of the dispersed phase (gas phase) in volume V^1. Unlike a continuum, the volume fraction cannot be defined at a point. Equivalently, the volume fraction of the continuous phase is:

$$\alpha_f = 1 - \alpha_g \tag{1.2}$$

This volume fraction is sometimes referred to as the void fraction and in the chemical engineering literature, the volume fraction of the gas phase is often referred to as *gas holdup*.

---

[1]The volume V^0 is the limiting volume that ensures a stationary average.

1.2.2 Superficial and phase velocities

For multiphase flow in a pipe, the superficial velocity of each phase is the mass flow rate G_k, of kth-phase, divided by the pipe area A_{pipe} and material density ρ_k.

$$j_k = \frac{G_k}{\rho_k A_{pipe}} \tag{1.3}$$

In other words, it is the velocity of the phase if the phase occupies the whole pipe area. This is an essential parameter for the formulation of drift-flux models.

The phase velocity v_k is the actual velocity of the phase. The superficial velocity and the phase velocity are related by the volume fraction:

$$j_k = \alpha_k v_k \tag{1.4}$$

1.2.3 Hydraulic diameter, D_h

The hydraulic diameter is important to describe the geometry of a system and the flow regimes and its dimensionless values can be used to distinguish the *type of pipe* (i.e. small, intermediate and large). When the hydraulic diameter of a two-phase flow channel reaches a certain size, slug bubbles bridging the entire diameter can no longer be sustained due to Taylor instability. For this reason Mishima and Ishii [10] defined the critical diameter at which this occurs in terms of the Taylor wavelength as:

$$D_h^* = \frac{D_h}{\sqrt{\frac{\sigma}{g \Delta \rho}}} \geq 30 \tag{1.5}$$

When the pipe diameter is larger than this value, this results in dramatic changes in the structure and dynamics of the two-phase flow.

1.2.4 Surface tension (σ) and Liquid viscosity (μ_f)

The effect of surface tension is important for the analysis of interfacial stability and of flow regimes: it makes all dynamical problems nonlinear.

The liquid-phase viscosity have a significant effect on the hydrodynamic characteristics of two-phase flows. An increase in viscosity results in a stable bubble interface and thereby results in an increase in coalescence rate and decrease in breakup rate.

1.2.5 Temperature and pressure

The effect of temperature can be accounted for by the change in physical properties of fluids. In the case of air and water at standard temperature and pressure, the density of the two phases differs by a factor of about 800 (similar differences are typical of water liquid/water vapor densities).

1.2.6 Bubble size

This has a very important effect on the transport coefficients, because the shape and the size of an object is one of the primary determinants of the hydrodynamic force, the heat, and the mass transfer coefficients. The parameters that determine the size and shape are: the bubble velocity, the density of the fluids, the viscosity of the fluids, the surface tension, the gravitational acceleration. Two independent dimensionless groups can be used to describe the shape of bubbles:

- Eötvös number ($Eo = \frac{\Delta \rho g d_s^2}{\sigma}$);

- Morton number ($Mo = \frac{g \mu_f^4 \Delta \rho}{\rho_f^2 \sigma^3}$).

The bubble diameter (d_s) should be expressed by the *Sauter mean diameter*, which is defined as the diameter of a sphere that has the same volume/surface area ratio as a particle of interest.

$$d_s = \frac{\int_{x_{min}}^{x_{max}} x^3 f(x) dx}{\int_{x_{min}}^{x_{max}} x^2 f(x) dx} \qquad (1.6)$$

When x is the diameter, $f(x)$ is the probability density function of the bubble diameter, x_{min} and x_{max} are the minimum and maximum observed diameter, respectively.

If we are assuming a spherical bubble shape, the specific gas-liquid interfacial area is related to the void fraction and the sauter mean diameter. Therefore, a precise knowledge of the global void fraction and bubble size distribution is needed to determine the specific gas-liquid interfacial area.

1.3 Two-phase flow governing equations

In general, a two-phase flow can be considered as a field that is subdivided into single-phase regions with moving boundaries between the phases. The equations that describe each subregion are the standard differential balance equations and an appropriate boundary jump conditions must be used to match the single-phase equations. This formulation would result in a multi-boundary problem with the positions of the interface being unknown due to the coupling of the fields and the boundary conditions. Mathematical difficulties encountered by using this local instant formulation may be insurmountable and, very often, rarely needed for a practical engineering problems. The solution is an appropriate averaging of these equations (in form of the *local instant formulation*) to bring the problem at the macro-scale.

1.3.1 Problem of the local instant formulation

The local instant formulation is the starting point to derive the equations need to describe a complex physical system, this includes: the derivations of field equations, constitutive equations, and interfacial conditions. With this kind of formulation, it can be described the separated flows, the energy and mass exchange and the bubble dynamics. The mathematical difficulties encountered with this formulations stem from:

1. Multiple deformable moving interfaces causes complicated coupling between the field equations of each phase and the interfacial conditions;

2. The turbulence and the motions of the interfaces introduces instabilities and interfacial waves;

3. Significant discontinuities of properties at interface introduces huge local jumps in various variables in space and time.

Most two-phase flow observed in practical engineering systems have extremely complicated geometries and motions and it is not possible to solve local instant motions of the fluid particles.

The averaging procedure can be considered as "low-pass filtering", excluding unwanted high frequency signals from local instant fluctuations. It is important to remember that the turbulence, which influence the macroscopic phenomena, should be taken into account with proper correlations. By averaging methods it can obtain the mean values of fluid velocities and physical proprieties.

1.3.2   Averaging methods

Averaging procedures can be classified into three main groups:

1. Eulerian averaging;

2. Lagrangian averaging;

3. Boltzmann statistical averaging.

The most important and widely used group of averaging in continuum mechanics is the *Eulerian averaging*, because it is closely related to human observations and most instrumentation. The basic concept underlining this method is the time-space description of physical phenomena. In the Eulerian description, the time and space coordinates are taken as independent variables and various dependent variables express their changes

with respect to these coordinates. These averaging processes are basically integral operators, therefore, it has an effect of smoothing the instant (or local) variations within a domain of integration.

The *Lagrangian averaging* is naturally fitted to a study of the dynamics of a particle. If the interest is focused on a behavior of an individual particle, the Lagrangian average is important and useful for analyses. The Lagrangian mean values are directly related to the Lagrangian description of mechanics.

The *Boltzmann statistical averaging* with a concept of the particle number density is important when the collective mechanics of a large number of particles are in question. As the number of particles and their interactions between them increase, the behavior of any single particle becomes so complicated and diversified, it is not practical to solve for each particle. In such a case, the behavior of a group of many particles increasingly exhibits some particular characteristics that are different from a single particle as the collective particle mechanics becomes a governing factor.

The applications of averaging can be divided into two main categories:

1. To define properties and then to correlate experimental data;

2. To obtain usable field and constitutive equations that can be used to predict macroscopic processes.

The most elementary use is to define mean properties and motions that include various kinds of concentrations, density, velocity and energy of each phase or of a mixture. These properly defined mean values then can be used for various experimental purposes and for developments of empirical correlations. The choice of averaging and instrumentation are closely coupled since, in general, measured quantities represent some kinds of mean values themselves.

The Eulerian area averaging over a cross section of a duct is very useful for engineering applications, since field equations reduce to a one-dimensional model. By area averaging, the information on changes of variables in the direction normal to the main flow is basically lost. Therefore, the transfer of momentum and energy between the wall and the fluid should be expressed by empirical correlations or by simplified models

which replace the exact interfacial conditions. The rational approach to obtain a one-dimensional model is to integrate single-phase differential field equations over the cross sectional area.

1.4 Drift-flux model approach

A general two-phase flow problem can be formulated by using a two-fluid model or a drift-flux model, depending on the degree of the dynamic coupling between the phases. In the two-fluid model, each phase is considered separately and the model is formulated in terms of two sets of conservation equations governing the balance of mass, momentum, and energy of each phase. The two-fluid model is more accurate than the drift-flux model, but it is also much more computationally intensive. The drift-flux model remains one of the best available ways to quickly estimate the void fraction in a two-phase system. In addition, the one-dimensional form of the two-fluid model requires a drift-flux like constitutive relation to calculate the area-averaged relative velocity in the calculation of the interfacial drag.

The Drift-flux model (first developed by Zuber and Findlay [13] in '60s) consider the mixture as a whole, rather than two phases separately and it takes its name from the drift-flux term, v_{gj} which is the relative velocity between gas and the volumetric flux of the whole mixture. This formulation requires some drastic constitutive assumptions causing some of the important characteristics of two-phase flow to be lost. This approach is appropriate for modeling the dynamics of two components when they are closely coupled. If the axial dimension of the systems is great enough to ensure sufficient interaction times, the drift velocity between phases can be formulated as well as rigorous drift-flux formulation, because there is a sufficient volume to ensure a good statistical average of the physical proprieties. So, the drift-flux model can be applied in many practical engineering systems even when two-phase mixtures are weakly coupled locally. The usefulness of the drift-flux model in many practical engineering systems comes from the fact that even two-phase mixtures that are weakly coupled locally can be considered coupled, because the relatively large axial dimension of the systems usually gives sufficient interaction times. The most important aspect of the drift-flux model is the reduction in the total number of field and constitutive equations required in the

formulation in comparison with the two-fluid model, because only four field equations are necessary:

- The mixture continuity equation;

- The gas phase continuity equation;

- The momentum equation;

- The energy equation.

The relative motion between phases and the other constitutive relations must be expressed by additional constitutive equations, that replace the dynamic interaction relations, because one of the two momentum equations has been eliminated from the formulation.

1.4.1 One-dimensional drift-flux model

The three-dimensional drift-flux equations are, as the two-fluid model, rather complex and would require a computer and several constitutive relations for resolve them properly. With averaging methods it's possible to derive the one-dimensional drift-flux equations.

The Mixture Continuity Equation:

$$\frac{\partial \rho_m}{\partial t} + \nabla \cdot (\rho_m \mathbf{v_m}) = 0 \tag{1.7}$$

The Continuity Equation for gas-phase:

$$\frac{\partial \alpha_g \rho_g}{\partial t} + \nabla \cdot (\alpha_g \rho_g \mathbf{v_m}) = \Gamma_g - \nabla \cdot \left(\frac{\alpha_g \rho_g \rho_f}{\rho_m} \mathbf{v_{gj}} \right) \tag{1.8}$$

The rational approach is to integrate the three-dimensional drift-flux model over a cross-sectional area and then introduce proper mean values. To achieve this scope, the area average over the cross-sectional area and the void-fraction-weighted mean value are employed.

10

$$\langle F \rangle = \frac{1}{A} \int_A F dA; \quad \langle\langle F_k \rangle\rangle = \frac{\langle \alpha_k F_k \rangle}{\langle \alpha_k \rangle} \tag{1.9}$$

The effects of non-equilibrium are accommodated in the drift-flux model by a constitutive equation for phase change. Since the rates of mass, energy and momentum transfer at the interfaces depend on the structure of interface, these constitutive equations are functions of flow regimes. The transfer of momentum and energy between the wall and the fluid should be expressed by empirical correlations or by simplified models.

By area-averaging Eqs. (1.7) – (1.8) and considering the *x-coordinate* the mono-dimensional direction, using the various mean values, we obtain: the mixture continuity, the gas-phase continuity, the mixture momentum and the energy equations for 1D averaged drift-flux model.

The averaged Mixture Continuity Equation:

$$\frac{\partial \langle \rho_m \rangle}{\partial t} + \frac{\partial}{\partial x}(\langle \rho_m \rangle v_m) = 0 \tag{1.10}$$

The averaged Continuity Equation for gas-phase:

$$\frac{\partial \langle \alpha_g \rangle \rho_g}{\partial t} + \frac{\partial}{\partial x}(\langle \alpha_g \rangle \rho_g v_m) = \langle \Gamma_g \rangle - \frac{\partial}{\partial x}\left(\frac{\langle \alpha_g \rangle \rho_g \rho_f}{\langle \rho_m \rangle} v_{gj} \right) \tag{1.11}$$

We note here that the effects of the mass, momentum, and energy diffusion associated with the relative motion between phases appear explicitly in the drift-flux formulation, since the convective terms on the left-hand side of the field equations are expressed in terms of the mixture velocity. These effects of diffusions in the present formulation are expressed in terms of the drift velocity of the dispersed phase v_{gj}.

$$v_{gj} = v_{gj}(\langle \alpha_g \rangle, \langle p_m \rangle, g_x, v_m, etc.) \tag{1.12}$$

To take into account the mass transfer across the interfaces, a constitutive equation for Γ_g should also be given in a functional form.

$$\langle \Gamma_g \rangle = \langle \Gamma_g \rangle \left(\langle \alpha_g \rangle , \langle p_m \rangle , \frac{\partial \langle p_m \rangle}{\partial t}, v_m, etc. \right) \tag{1.13}$$

1.4.2 Closure models for drift velocity and distribution parameter

The velocities based on the center of mass (v_k) are important for dynamic analyses because of the fundamental theorem of center of mass. The velocities based on the center of volume (j_k), namely, volumetric fluxes, are useful for kinematic analyses. This is particularly true if each phase has constant properties. To obtain the kinematic relation between the two fluids, we start from the definition of the drift velocity: the relative velocity between the gas and the entire mixture:

$$v_{gj} \equiv v_g - j \tag{1.14}$$

Next is to apply the void fraction averaging (Eqs. (1.9)) at the gas velocity, substitute the above equation and multiply all with the averaged volumetric flux:

$$\langle \langle v_g \rangle \rangle = \frac{\langle \alpha v_g \rangle}{\langle \alpha \rangle} = \frac{\langle \alpha (v_{gj} + j) \rangle}{\langle \alpha \rangle} \cdot \frac{\langle j \rangle}{\langle j \rangle} \tag{1.15}$$

All velocities are the components in the axial direction. Introducing the definitions of v_{gj} and C_0:

$$\begin{cases} C_0 = \dfrac{\langle \alpha j \rangle}{\langle \alpha \rangle \langle j \rangle} \\ \langle \langle v_{gj} \rangle \rangle = \dfrac{\langle v_{gj} \alpha \rangle}{\langle \alpha \rangle} \end{cases} \tag{1.16}$$

We found the well-know equation of Drift- flux model [13]:

$$\langle \langle v_g \rangle \rangle = \frac{\langle \alpha v_{gj} \rangle}{\langle \alpha \rangle} + \frac{\langle \alpha j \rangle}{\langle \alpha \rangle} \cdot \frac{\langle j \rangle}{\langle j \rangle} = C_0 \langle j \rangle + \langle \langle v_{gj} \rangle \rangle \tag{1.17}$$

Evaluating these quantities requires knowledge of the velocity and void distributions within the flow. Generally this information is not available, so constitutive relations are

relied on to predict C_0 and V_{gj}, and thereby estimate the void fraction and gas velocity. The factor C_0 is known as a distribution parameter. Physically, this effect arises from the fact that the dispersed phase is locally transported with the drift velocity v_{gj} with respect to local volumetric flux j and not to the average volumetric flux $\langle j \rangle$. For example, if the dispersed phase is more concentrated in the higher-flux region, then the mean transport of the dispersed phase is promoted by higher local j. The value of C_0 can be determined from assumed profiles of the void fraction α_g and total volumetric flux j, or from experimental data (i.e. by assuming power-law profiles in a pipe for j and α_g).

If the concentration profile is uniform across the pipe, then the value of the distribution parameter is equal to unity. In addition, if the effect of the local drift v_{gj} is negligibly small, then the flow becomes essentially homogeneous. In this case, the relation between the mean velocity and flux is directly proportional. The deviation of the experimental data from direct proportionality shows the magnitude of the drift of the dispersed phase with respect to the volume center of the mixture.

In a practical way, in order to found the coefficients of Drift-flux model (C_0 and v_{gj}), it can be plotted the gas velocity (v_g) against the volumetric flux (j). An important characteristic of this kind of plot is that, for two-phase flow regimes with fully developed void and velocity profiles, the data points cluster around a straight line. This trend is particularly pronounced when the local drift velocity is constant or negligibly small. Hence, for a given flow regime, the value of the distribution parameter may be obtained from the slope of these lines, whereas the intercept of this line with the mean velocity axis can be interpreted as the weighed mean local drift velocity (see Fig. 1.1).

The extensive study by Zuber and Findlay [13] shows that C_0 depends on pressure, pipe geometry, and perhaps flow rate. Here, a simple correlation for the distribution parameter in bubbly-flow regime is presented based on study by [4]. First, by considering a fully developed bubbly flow, we assumed that C_0 depends on the density ratio ρ_g, ρ_f and on the Reynolds number based on liquid properties (calculated with: the total mass flow rate, the hydraulic diameter, and the viscosity of the liquid).

$$C_0 = C_0 \left(\frac{\rho_g}{\rho_f}, \frac{GD_h}{\mu_f} \right) \tag{1.18}$$
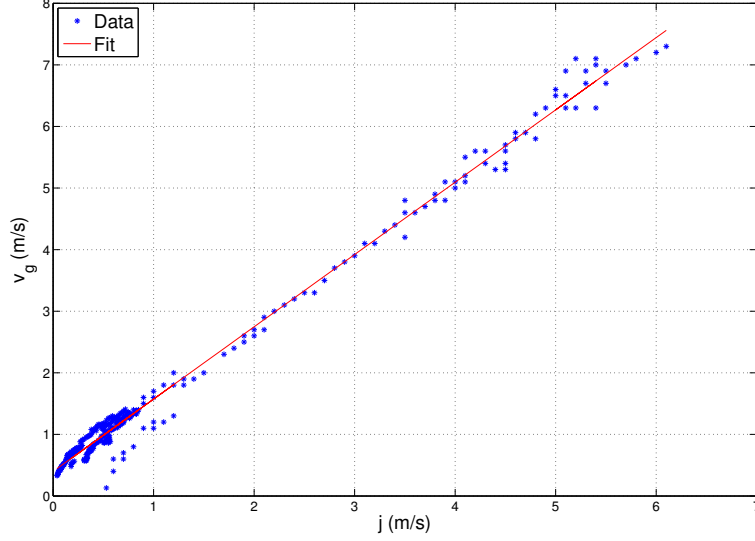
FIGURE 1.1: Method for recognize the coefficients of Drift-flux models with Hill's data [6]

A single-phase turbulent-flow profile and the ratio of the maximum velocity to mean velocity give a theoretical limiting value of C_0 at $\alpha_g \to 0$ and $\rho_g/\rho_f \to 0$, since in this case all the bubbles should be concentrated at the central region.

$$C_\infty = \lim_{\alpha_g \to 0} \frac{\langle \alpha_g j \rangle}{\langle \alpha_g \rangle \langle j \rangle} \tag{1.19}$$

Based on these limits and various experimental data in a fully developed flow, the distribution parameter can be given approximately by:

$$C_0 = C_\infty - (C_\infty - 1)\sqrt{\frac{\rho_g}{\rho_f}} \tag{1.20}$$

where the density group scales the inertia effects of each phase in a transverse void distribution.

Physically, Eq. (1.20) models the tendency of the lighter phase to migrate into a higher-velocity region, thus resulting in a higher void concentration in the central region. Over a wide range of Reynolds number, Eq. (1.19) can be approximated by $C_\infty \approx 1.2$ for a

flow in a round tube. Furthermore, for a rectangular channel, the experimental data show this value to be approximately 1.35.

There are many type of constitutive equations for the one-dimensional drift-flux model for various flow conditions:

- for upward bubbly flow;

- for upward adiabatic annulus and internally heated annulus;

- for downward two-phase flow;

- for bubbling or boiling pool systems;

- for large diameter pipe systems;

- for reduced gravity conditions;

- for rod bundle geometry;

- for pool rod bundle geometry.

For example, in this thesis, we are interested on the constitutive equations for large diameter pipe systems. So, the distribution parameter and the drift velocity, obtained by the graphical method, may not reflect the reality of the flow. Based on the definitions of the distribution parameter and the average drift velocity, it is possible to obtain the local C_0 and the v_{gj} from the radial distribution of void fraction, gas velocity and liquid velocity measured by an experimental procedures.

In the state-of-the-art section (4.1), many constitutive equations have been collected for vertical upward two-phase flows in conventional diameter round tubes of small size and large size, under relatively high flow rate conditions. In order to improve the prediction accuracy and range, in various two-phase flow transient analyses, it has been required to develop precise constitutive equations for downward flow and counter-current flows. Clark and Flemmer [8] concluded that the vertical pipe's drift-flux model is applicable to downward flow as well.

For most practical two-phase flow problems, and if the transverse pressure gradient within a channel is relatively small, the density of each phase (gas and liquid) within

any cross-sectional area is considered to be uniform, so that $\rho_k = \langle\langle\rho_k\rangle\rangle$. Additionally, in the following analysis, we will omit the bracket notation, that means area-average operator.

Under these assumption, the average mixture density is given by:

$$\rho_m = \alpha_g\rho_g + (1 - \alpha_g)\rho_f \tag{1.21}$$

The axial component of the weighted mean velocity of kth-phase is:

$$v_k = \frac{\langle\alpha_k v_k\rangle}{\langle\alpha_k\rangle} = \frac{j_k}{\alpha_k} \tag{1.22}$$

Then the mixture velocity is defined from a fraction of the gas phase momentum referred to whole momentum and the continuity axiom[2] is:

$$v_m = \alpha_g\frac{\rho_g}{\rho_m}v_g + (1 - \alpha_g)\frac{\rho_f}{\rho_m}v_f \tag{1.23}$$

The mixture volumetric flux is given by the sum of the dispersed phase's volumetric flux and the continued phase's volumetric flux, that are related with the *real* velocities by the void fraction.

$$j = j_g + j_f = \alpha_g v_g + (1 - \alpha_g)v_f \tag{1.24}$$

The *drift velocity* (1.25) has a similar role as the diffusion coefficient have in single-phase equations, but differently, as it plays on a macro scale level. Therefore, the drift velocity is strongly dependent on the flow regime.

$$v_{gj} = v_g - j = (1 - \alpha_g) \cdot (v_g - v_f) \tag{1.25}$$

---

[2]The velocity fields are expressed in terms of the mixture (center-of-mass) velocity, in order to preserve the additive characteristic of the extensive variables.

The experimental determination of the drift velocity is possible if the volume flow rate of each phase, Q_k, and the mean void fraction α_g are measured. The Eq. (1.25) can be transformed into Eqs. (1.26) with Eq. (1.23) and Eq. (1.21).

$$
\begin{cases}
v_f = v_m - \left(\dfrac{\rho_g}{\rho_m}\right)\left(\dfrac{\alpha_g}{1 - \alpha_g}\right) v_{gj} \\[2ex]
v_g = v_m + \left(\dfrac{\rho_f}{\rho_m}\right) v_{gj}
\end{cases}
\tag{1.26}
$$

From Eq. (1.24) and Eqs. (1.26), we can derive the last important relation that solve the problem of drift-flux for α_g and v_m with a given constitutive relation for v_{gj}.

$$
j = v_m + \frac{\alpha_g}{\rho_m}(\rho_f - \rho_g)v_{gj}
\tag{1.27}
$$

1.5 Measurement techniques for two phase flow

The measurement techniques are subdivided in four groups, based on the complexity:

1. Visual observation

2. Evolution of global hydrodynamic parameter

3. Temporal signatures of quantity related to hydrodynamics

4. Advanced measurement techniques

In general, the choose between two measuring instrumentation may be balanced between the accurate insight into the mechanics of the flow and the possibility that such intrusive instrumentation may alter the development of the flow. If a measurements are being made at several axial locations simultaneously, it was desirable to use a non-intrusive method so that the development of the flow could be observed.

1.5.1 Visual observation

The visual observation is the simplest method to study the flow patterns. When the radial dimension (or diameter, for circular pipes) is too big, this method is useless to catch the fluid dynamics in the pipe center. It can be made with the support of a camera that can store the photos for a subsequent post-processing. In the homogeneous regime, slow and vertically rising bubbles can be easy observed. In the heterogeneous regime there is an intense interaction of bubbles and the visualization is more difficult. In the Fig. 1.2 you can see the differences summarized above.

(a) Low air flow rates $(20 N \mathrm{dm}^3 \min^{-1})$

(b) High air flow rates $(340 N \mathrm{dm}^3 \min^{-1})$
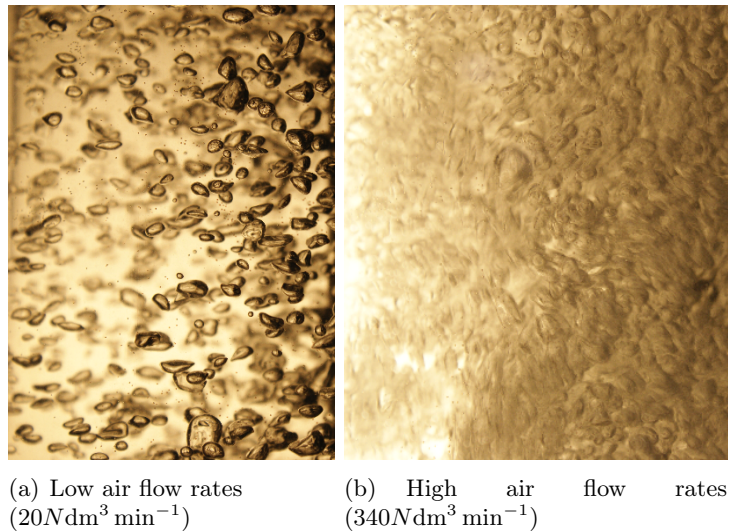
FIGURE 1.2: Flow patterns of our experimental facility

1.5.2 Evolution of global hydrodynamic parameters

The evolution of global hydrodynamic parameters is a manifestation of the prevailing flow patterns and variation of the regimes. They are been utilized to identify flow regime transition point. Typically, the global hydrodynamic parameters have been quantified based on overall gas holdup. For example, if you want to calculate the gas void fraction in a section of the test facility you can set two pressure transducers at two different heights and, then, use this equation to found the averaged gas holdup.

$$\alpha = \frac{\Delta p}{\rho g \Delta h} \tag{1.28}$$

1.5.3 Temporal signatures of quantity related to hydrodynamics

The temporal signatures of quantity related to hydrodynamics represent macroscopic phenomena that are result of prevailing microscopic phenomena. The temporal signatures, utilized for flow regime transition are: pressure fluctuations, local holdup fluctuations using resistive or optical probes, temperature fluctuations, local bubble frequency, conductivity probe, sound fluctuations. Below, few instrumentations are described.

1.5.3.1 Electrical impedance void meters

An impedance void meter is a non-intrusive conductance type probe that relies on the different conductivity properties between air and water of the two-phase mixture in the measurement area, which is recorded as a voltage output from the impedance meter circuit; it allows very accurate measurement of the void fraction without the use of intrusive techniques. The actual relationship between void fraction and output voltage is relatively complex and depends on the flow pattern. The sensor thickness was chosen so as to be larger than the dimension of a typical bubble, yet shorter than the length of a cap or a slug bubble.

Thus each instrument is cross-calibrated against the void fraction measured by differential pressure. The cross-calibration is performed at very low liquid velocity where the frictional pressure drop, calculated using dedicated models, is less than 2% of the total pressure drop. For this reason, the accuracy of the impedance probe calibration is dependent on the accuracy of the pressure transducers used in the calibration and the electrical properties of the circuit. Overall, the relative error in the void fraction measurements is less than 10% of the measured value for void fractions between 0.2 and 0.4 and less than 5% for void fractions above 0.4 [14].

1.5.3.2 Four-sensor electrical conductivity probes

The four-sensor electrical conductivity probe was first developed by Isao and Mamoru [15] and it has been one of the most widely used instruments for local measurements

TABLE 1.1: The measurement uncertainty of conductivity probes

Measurement uncertainty	Details	Uncertainty
Probe structure	interface velocity, probe geometry, measurement frequency and response time	10.3%
Deformation of bubble	–	11.9%
Variations on electronic signal	uncertainty in the residence time of each bubble	10%

in gas-liquid two-phase flow experiments. It uses the conductive properties of air and water to determine when each of the four sensors is surrounded by air or water.

A multi-sensor conductivity probe is capable of measuring the local interfacial velocity of individual bubbles and thereby determines the local time-averaged interfacial area concentration, interface velocity, bubble residence time and the bubble chord length. The measurement uncertainties are reported in table 1.1.

1.5.3.3   Optical fibre probes

This instrument is used in our facility to collect the local data of void fraction and other parameter included bubble distribution used for the drag law in two-fluid model (see section 3.3.2).

The working principle of an optical probe is based on the refraction and reflection laws in the optical fiber. A light source emits pulses, which run inside an optical fiber. The fiber tip, often made in sapphire to be more robust, is designed to exploit refraction laws at the interface with the surrounding medium. It may be conical or with more complex shapes, e.g. conical-cylindrical-conical. When the probe tip is immersed in water, the light pulse leaves the fiber and is lost; otherwise it is reflected back, modified only in phase, along the fiber. A photodiode registers the returned pulses and emits a voltage signal, which is then amplified and processed. Single or double threshold filtering returns a binary signal which represent the phase density function and whose average gives an estimate of the local void fraction. The interference frequency can also be extracted, so that – with the support of statistical assumptions about to flow – some insight about the local area concentration can be gained.

Using optimized probes, the probe signal can be further processed to extract information about the flow velocity too. The same information can be obtained using double-tip probes, by cross-correlation of the signals acquired by the two probe tips. Concerning limitations of such techniques, the stem of the probe is designed not to influence the fluid-dynamics of the mixture, but the tip of the probe can deflect, warp and decelerate the flow structures, particularly small bubbles. An underestimation of the time of residence of the gaseous phase may occur due to the so-called blinding and drifting effects, while the crawling effect may cause an overestimation of the same. As for the time aspects, each sampling can be considered instantaneous compared to the characteristic times of the phenomenon, but for fast flows the sampling frequency may be too low, so that small flow structures may pass without being "seen" by the probe. Based on the basic working principle of the optical probe and the definition of various local two-phase flow parameters, the optical four-sensor probe can measure reliably the values of:

1. The time-averaged local void fraction;

2. The time-averaged local interfacial area concentration;

3. The average local gas velocity (v_g);

4. The time-averaged local Sauter mean diameter (D_{sm}).

In order to verify the accuracy of the local four-sensor probe measurements, the area-averaged quantities obtained by integrating the local flow parameters over the flow channel were compared with those measured by other cross-calibration methods such as the differential pressure gauges for void fraction and the orifice flow meters for superficial gas velocity. The averaged and maximum relative deviations of the area-averaged void fractions between the four-sensor probe measurements and the differential pressure gauge measurements are between 5% and 15% [16].

1.5.3.4 Wire mesh sensor

The wire mesh sensor can rapidly measure the gas profiles and has been used to visualize the internal structure of flow in large pipes. The operating principle of the wire mesh

technique is based on a considerable difference in the electrical conductivities of the fluid pair employed. The wire mesh sensor yields a sequence of instantaneous conductivities in each junction formed by a pair of crossing wires. This configuration tends to distort cap bubbles at low liquid velocities. For each measuring location, the instantaneous gas fraction is determined by relating the two-phase conductivity to the reference signal for the liquid phase only. This gives a three-dimensional matrix of void fractions. During signal acquisition, voltage pulses are supplied successively to activate the transmitter wires or electrodes. The resulting current at the receiver wire due to this transmission is a measure of the fluid conductivity in the control volume surrounding the junction of the two wires. The reported accuracy of the wire mesh sensor was about 5% [14].

1.5.4 Advanced measurement techniques

The advanced measurement techniques are based on various imaging and velocimetric techniques: Particle Image Velocimetry (PIV), Electrical Capacitance Tomography (ECT), Electrical Resistance Tomography (ERT), Laser Doppler Anemometry (LDA), Computer Automated Radioactive Particle Tracking (CARPT), Computed Tomography (CT), Gamma Densitometry (GD).

1.5.4.1 Gamma densitometry [1]

The gamma densitometers employ a Cs_{137} radioactive source that emits gamma rays on one side of the pipe to be picked up on the other side by an ionization type detector. As the gamma rays are attenuated differently in gas and liquid, the radiation intensity at the detector depends on the phase distribution in the pipe. With the signals for pure gas and liquid as reference points, the densitometers give a direct measure of the ray path occupied by liquid or gas.

1.5.4.2 Laser Doppler Anemometry [2]

To measure the axial velocity component in the gas phase, the Laser Doppler Anemometry can be used. It is a measurement technique which has the advantage of not disturbing the flow and to relatively allow measurements close to the gas-liquid interface.

Two beams from a He-Ne laser are crossed to produce a very little measurement volume. Two laser beams which are reflected by small particles are used in the flow, passing through the measuring volume of the LDA and received by a photodetector. A beat frequency contained in the reflected beams is used to determine the velocity.

1.5.4.3 Particle Image Velocimetry [3]

In PIV the continuous phase is seeded with small tracer particles that ideally follow the flow, which are already present in tap water. A laser is used to illuminate the tracer particles in a cross section of the flow. Then two subsequent images with a short exposure time delay are recorded with a digital camera. These images are divided into small interrogation areas. Each interrogation area in the first image is then correlated with the corresponding interrogation area in the second image. In the resulting correlation function a distinct peak can be found. The location of the peak corresponds to the displacement of the particles in the interrogation area. The velocity is determined by dividing the measured displacement by the exposure time delay. The advantage of PIV are that velocities of two different phases can be determined simultaneously in a whole plane in the flow, without disturbing the flow. One of the major disadvantages of these techniques is the rather low temporal resolution.

1.6 Data processing techniques

To determine the flow regime from a voltage signal, a neural network classification system can be used. When a sensor is coupled with a properly trained Self-Organized Map or neural network, it can provide nearly instantaneous flow regime information while using a very small amount of computing power and it is possible to employ a control systems. A neural network is a simulated group of interconnected artificial neurons intended to simulate the function of the human brain on a limited scale. In the self-organized approach, at the neural network is given a number of sample data sets and told to group them into several categories. The network then trains itself using these sample sets to recognize the most significant features of the data sets and correctly categorize the inputs. The inputs to the neural network are the mean and standard deviation of the void fraction signal from an electrical signal.

Schlegel et al. [14] used three neural networks, each one is trained using one-third of the experimental data, then each network is used to categorize the remaining data into the selected flow regimes. In this way, each data point is classified twice to confirm the categorization. The result of the neural network flow regime identification process is a number associated with each input that corresponds to the category number which that data point was assigned to. These numbers are then associated with the flow conditions for each experiment to create the flow regime map.

Some statistical parameters, of the instantaneous void fraction signal, can be used to characterize the flow regime in a neural network system. The various parameters must first be properly scaled to ensure that their influence is correctly weighted, because is necessary to prevent one parameter from dominating the classification scheme and skewing the results.

- Mean;

- Standard deviation;

- Skewness.

The trends in the standard deviation and the skewness, can indicate the transitions between the flow regimes.

Chapter 2

TWO-PHASE FLOW IN VERTICAL PIPES

In this chapter will be treated the two-phase flow in the vertical pipes. The flow patterns and the regime transitions are reported and described for all types of facility. A review of the state-of-the-art of drift-flux models is reported and will be used to perform the two models in this thesis.

2.1   Small and Large pipes

In literature certain geometries, such as small pipes, have been rigorously investigated. On the other hand, fewer studies are found regarding large diameter pipes, mainly because large geometries can be too large and complex to build instead the small pipes. If the systems include flow channels of large diameter, instead of small pipes, must be developed ad hoc experimental data and correlations. In addition, the ability to accurately identify the flow regimes and characterize the physical mechanisms governing each flow regime is necessary for the development of accurate two-phase flow models.

In order to classify the pipe dimension, a dimensionless parameter, related to the hydraulic diameter, has been introduced [10] and permits to identify a boundary between small and large pipes. Ishii defined the critical diameter for this boundary, in terms of the Taylor wavelength as Eq. (2.1). Above this value the pipe can be considered *large*

and below, *small*. In reality there is a range where the pipe show both peculiarity of small and large, called *intermediate*, between $18.6 < D_h^* < 30$.

$$D_h^* = \frac{D_h}{\sqrt{\frac{\sigma}{g\Delta\rho}}} = 30 \tag{2.1}$$

The characteristics and the flow regimes of two-phase flow in large pipes are much different than those in small pipes. Mishima and Ishii [10], firsts noted that the slug bubbles seen in small pipes were not seen in pipes above a certain diameter, and Taitel et al. [17] noted that the bubbly flow pattern does not exist under a critical diameter (Eq. (2.10)). For a large diameter system, the Taylor bubbles become unstable when they reach a certain diameter due to turbulent effects, and the Taylor bubbles are unable to form slugs instead of cap bubbles of various sizes. The experimental data obtained in small diameter pipes (in which slug flow exists) cannot be scaled for use in understanding flow in large diameter pipes. Any consideration about the large diameter pipes must take into account these effects:

Lack of slug bubbles. This means that the void fraction radial profile in large pipes will be very different from those of small pipes in the cap/slug flow regime.

Reduced influence of the pipe wall. It means that the relative velocity between the Taylor bubbles and liquid will be increased in comparison to small pipes.

Strong secondary recirculations in the flow and increased turbulence. The increased turbulence due to the flow of liquid around the cap bubbles results in the development of recirculation patterns, especially at lower liquid flow rates.

In the large diameter case, churn-turbulent flow is characterized by rapid formation and disintegration of large bubbles resulting in a very chaotic flow. These bubbles can also be affected by diffusion, as they are smaller than the pipe diameter, whereas churn-turbulent bubbles in small diameter channels cannot move laterally due to the restriction imposed by the pipe wall. In large diameter pipes, slug bubbles cannot remain stable and the thin liquid film around it may not exist. Because of this the upper surface of larger bubble in the churn-turbulent flow regime are not stable and the bubble shape will not remain similar to that in cap-bubbly flow.

Turbulence plays an important part in determining the void profiles (i.e. the wall-peaking or center-peaking). Large cap bubbles can enhance turbulent phenomena because of eddies created near bubble skirts. Increased turbulent diffusion for flows in large diameter pipes can reduce wall-peaking, because it overwhelms the lift force and the result is a much flatter void fraction profile. The turbulent intensity is much higher in large diameter channels than in small diameter channels, because the bubbles are more little that the radial extension; this turbulence can enhance bubble breakup.

Typically void profiles from small pipes shows wall-peaking behavior at lower void fraction and center-peaking behavior at higher void fractions, but flows in large pipes are typically developing flows while flows in small pipes are generally fully developed[1] [5].

Some experimental data seems to indicate that the recirculation effects may be more significant in the smaller pipe sizes very close to the boundary between large and small pipes and become less important as the pipe size increases.

2.2 Flow in vertical pipes

The knowledge of flow regime is of unique importance in understanding and analyzing two-phase flow. Theoretical predictions of flow regimes are essential for both the design as well as smooth and safe operations of plant equipment. The two-phase flow through a conduit is more complex compared to the hydrodynamics of only one fluid through the same conduit. This is because, during two-phase flow, the two phases can distribute themselves in a large number of spatio-temporal arrangements known as flow patterns or flow regimes. Any transport phenomenon during two-phase flow is strongly influenced by the existing flow regime. The parameters of a vertical two-phase flow are:

1. Pipe geometry;

2. Velocity of each phase;

---

[1]For large diameter pipes with $L/D_h < 12 - 15$ flow development may not be negligible when developing predictions for flow behavior.

3. Properties of each phase;

4. Direction of the flow with respect to gravity (up, down or inclined) and respect of the motion of the other phases (co-current or counter-current);

5. Effect of body, surface tension and buoyancy forces;

6. Effect of heat and mass transfer.

There are a variety of two-phase flows depending on combinations of two phases as well as on interface structures. Two-phase mixtures are characterized by the existence of one or several interfaces and discontinuities at the interface. First, the two-phase mixtures can classify according to the combinations of two phases: gas/solid, gas /liquid, liquid/solid.

The second classification based on the interface structures and the topographical distribution of each phase is far more difficult to make, since these interface structure changes occur continuously. The two-phase flow can be classified according to the geometry of the interfaces into three main classes: separated flow, transitional or mixed flow and dispersed flow.

The third class is characterized by the presence of both separated and dispersed flow, subdivided according to the phase of dispersion. We can distinguish into: bubbly, cap/slug, churn-turbulent and annular. In general, the structures of the bubbly and slug flow regimes observed in downward flow are different than that observed in the vertical upward ones, due to more precise the size, shape and motion of the gas phase in downward two-phase flow [18].

2.2.1 Flow regimes

The flow regimes are the classifications of the geometrical structures of flow, therefore, it is postulated that the flow structures should depend directly on the geometrical parameter such as the void fraction and interfacial area. Under steady state fully developed conditions, it may be assumed that there exists a unique relation between the void fraction and the superficial velocities.
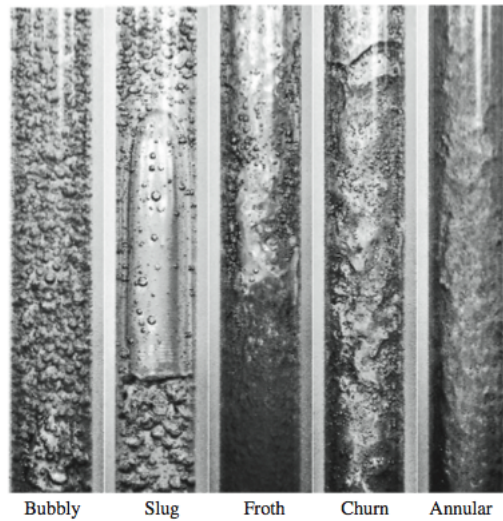
FIGURE 2.1: Flow patterns in vertical upward two phase flow from Godbole et al. [19]

The literature review (see section ??) shows that the major flow patterns observed in the vertical upward and downward two-phase flow are: bubbly, cap/slug, churn, falling film and annular flow.

2.2.1.1 Bubbly flow

The bubbly flow regime is characterized by the significant coupling between the two phases and consists of the gas as a discrete phase entrained into a continuous liquid phase. It occurs at low to moderate superficial gas velocities and it is characterized by uniformly sized small bubbles traveling vertically with minor transverse and axial oscillations. There is practically no coalescence and break-up, hence there is a narrow bubble size distribution. The gas holdup distribution is radially uniform; therefore bulk liquid circulation is insignificant. The size of the bubbles depends mainly on the nature of the gas distribution and the physical properties of the liquid.

2.2.1.2 Cap/Slug flow

For both vertical up and down flow the slug flow was observed to be characterized by the intermittent flow of the long elongated gas slugs. The slug diameter was found to be comparable to that of the pipe diameter.

In small pipes, most of the gas is located in large bullet shaped bubbles which have a diameter almost equal to the pipe diameter. Taylor bubbles are separated by slugs of continuous liquid which bridge the pipe and contain small gas bubbles. Between the Taylor bubbles and the pipe wall, liquid flows downward in the form of a thin falling film.

2.2.1.3   Churn flow

This regime occurs at high gas superficial velocities, due to intense coalescence and break-up. The non-uniform gas holdup distribution across the radial direction causes bulk liquid circulation. It is a highly disordered flow regime, in which the vertical motion of the liquid is oscillatory and a strong axial variation of the flow structure also occurs. It's much more chaotic, frothy and disordered than the slug flow. Typical of churn flow is this oscillatory or alternating direction of motion of the liquid.

2.2.1.4   Annular flow

The annular flow in both upward and downward flows is a separated type of flow with no direct coupling between the two phases. The gas core is surrounded by the continuous liquid film adjacent to the pipe wall. In annular flow, the gas flows along the centre of the tube. The liquid flows partially as a film along the walls of the tube and partially as droplets in the central gas core.

2.2.1.5   Falling film flow

Falling film flow is a unique type of flow that can be observed for low gas and liquid flow rates and appears only in vertical downward two phase flow. It is characterized by a wavy liquid film gliding down smoothly over the pipe surface and gas phase flowing through the core region.

2.2.2 Flow arrangements

The flow arrangement depend on the setting and configuration of each facility. The difference between every configuration has important consequences on the flow development and on the flow structure that we can observe. In fact, there are some flow regimes that we can not be observed in downward configuration instead of upward configuration (i.e. falling film flow and stalactite flow pattern [18]).

2.2.2.1 Upward flows

In vertical upward flow the liquid inertia and the buoyancy force on the gas phase act in the same direction of the mean flow, in other words the liquid inertia assists the gas bubbles to rise in the vertical upward direction resulting into the increased velocity of the gas bubbles with the increase in liquid and gas flow rates. The bubbles size increasing due to the reduction in the hydrostatic pressure and hence the expansion of the bubble volume.

Bhagwat and Ghajar [18] observed that at a constant gas flow rate the length of the Taylor slug and the slug rise velocity decreased with increasing liquid flow rate. They observed that the slugs due to their higher velocity push the liquid in front of them towards wall which falls as a film on the pipe surface. In the annular flow it was observed that the gas phase in the core region moves faster than that of the surrounding liquid film, and the gas flows through the core without any resistance offered by the liquid phase. The liquid phase being heavier than the gas phase is influenced by the gravity forces thus rendering into its slower velocity compared to the gas velocity.

For the drift-flux models' point of view, Bhagwat and Ghajar [18] observed that the correlations developed for vertical upward flow and based on the concept of the drift-flux model can be used to predict the void fraction for vertical downward orientation by flipping the sign of the drift velocity from positive to negative assuming the phase velocities to be positive in the flow direction.

2.2.2.2   Downward flows

In contrast to vertical upward two-phase flow, in the downward configuration the liquid inertia and the buoyancy force act in the direction opposite to each other and thus the gas phase resists the liquid flow. With increasing gas and liquid flow rates, as a consequence of the balance between the buoyancy and inertia forces both ends of the gas slug appeared flat. For the further higher gas and liquid flow rates and hence due to the dominant liquid inertia force, the gas slug was observed to be flowing with the bubble nose pointing in the vertical downward direction. In the annular regime, the liquid moves faster under the influence of gravity and high inertia in comparison to the gas phase.

For vertical downward flow the bubbles are observed to be concentrated in the near axis region of the pipe while the near wall region consisted of single phase liquid. This phenomenon is referred to as *coring* and is governed by the balance between the turbulent dispersion, lateral lift and wall repulsion forces [18]. Ghajar observed that at constant gas flow rate and with increasing liquid flow rates the dominant liquid inertia force shear down the bubbles, disintegrating them into smaller size bubbles and evenly distributing them across the pipe cross section. With increasing liquid flow rate, the gas bubbles increased in number, reduced in size and attained spherical shape. The increasing gas flow rate at constant liquid flow rate rendered the bubbles to elongate in the lateral direction and governed the transition from bubbly to the slug flow.

2.2.2.3   Counter-current flows

Counter-current flow phenomenon is characterized by the existence of a large relative velocity between the phases. At extreme values of relative velocity, this gives rise to instabilities. When the two fluids enter from two ends of the test section, there is a strong axial variation of the flow structure. Flooding phenomena can be observed at the extreme combinations of superficial velocities and is the main problem with this flow configuration. Annular flow has been observed for the combinations of either high air superficial velocities and low water superficial velocities or low air superficial velocities and high water superficial velocities.

2.2.3 Injection effect

In general, the effect of liquid and air injector design is very significant, even more in large pipe systems. In our experimental facility this not true, in particular at higher gas flow rate. The effect of the sparger is dominant in bubbly flow and diminishes as the system enters into churn-turbulent flow due to turbulence increasing. The bubble size in homogeneous flow is the direct result of the nature of distributor.

For large pipes it has been shown that the injection method, which influences the flow regime at the inlet of the region of interest, has a significant effect on the development of the flow. For this reason, Hibiki and Ishii [5] model is recommended for use in large pipes for bubbly: this is the only model that accounts for the effect of inlet flow regime for large pipes. In small pipes, such a complex model is not necessary because extensive experiments have been performed and none show dependence on the injection method.

2.2.4 Flow regime maps

Traditionally, flow regimes are identified from a flow-regime map obtained from experimental observations and/or theoretical laws (Fig. 2.2). The maps have the dimensional coordinates based on the liquid and gas superficial velocities or based on dimensionless groups.

The conventional flow regime maps are based on the liquid and gas superficial velocities. This approach may be suitable for slow transients and near fully developed conditions, where a mixture model such as the drift-flux model is sufficient. Under rapid transient conditions, the differences between traditional approach and transient conditions, maybe demonstrated by specially designed experiments. Nevertheless, no flow regime map is available that covers a wide range of industrial conditions.

An example of flow map is reported in Figure 2.2: the bubbly flow pattern can be found in zones I and II. In zone I to the left of curve A and below B, there are deformable bubbles which move upward with a zig-zag motion with Taylor-type bubbles occasionally appearing in the liquid. In zone II above curve B and to the left of C, one observes a more finely dispersed bubble system without any Taylor bubbles. To the
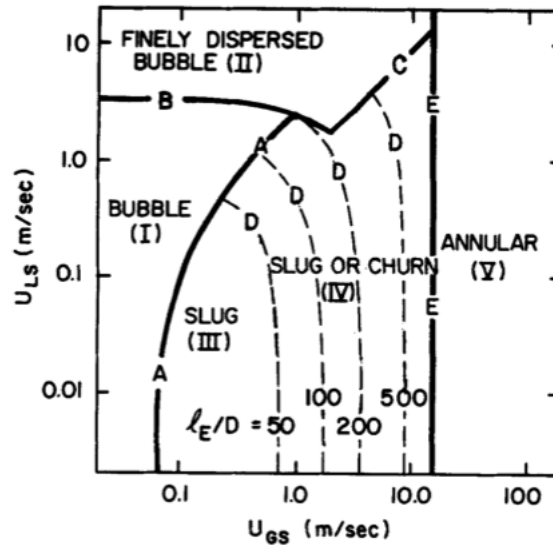
FIGURE 2.2: Flow pattern map from Taitel et al. [17]

right of A and below B in zone III, one expects to see the slug pattern. In the zone IV there is the churn pattern and on the right there is the annular zone (V).

2.3   Flow regime transitions

The demarcation of flow regimes becomes an important task in the design of two-phase components and has led to considerable research efforts, which have resulted into various experimental methods and empirical, semi-empirical and mechanistic models to identify flow regime transition. The flow regime transition depends, mainly, on:

1. Superficial volumetric fluxes of the two fluids;

2. Hydraulic diameter;

3. Liquid and gas phase properties;

4. Distributor design.

The flow regime criteria based on the superficial velocities of liquid and gas may not be consistent with the formulation of transients, because the void fraction can be uniquely

determined from the superficial velocities and the relative velocity. In the two-fluid model, the relative velocity is an unknown to be solved from the field equations and the void fraction cannot be determined uniquely from superficial velocities. Consequently, a flow-regime map based on superficial velocities alone may be unsuitable to the two-fluid model formulation. Therefore, a direct geometrical parameter such as the void fraction may be more suitable to use in flow regime criteria than the traditional parameters.

This difficulty does not arise in the drift-flux model because the constitutive relation for the relative velocity can be used to determine the void fraction. Below there are a description of the effects of operating parameters on flow regime transition [20]:

Effect of liquid height: due to gravity effect, an increase in liquid height decreases overall gas holdup due to high pressure that limiting the gas volume.

Effect of column diameter: overall gas holdup decreases with an increase in column diameter, up to a critical column diameter. Beyond a critical value of $D_h^* = 30$, column diameter has an insignificant effect on overall gas holdup.

Effect of operating pressure: an increase in pressure delays flow regime transition due to delays the appearance of large bubble.

Effect of surface tension: low concentration of surfactant stabilizes and high concentration destabilizes the homogeneous flow.

Effect of liquid viscosity: moderate viscosity destabilizes the homogeneous regime and advances the transition, low viscosity stabilizes the homogeneous regime.

Effect of temperature: an increase in temperature increases overall gas holdup due to the formation of small bubbles.

The predictions of flow regime transitions have been achieved by the development of various models and approaches.

It is essential to understand the physical mechanisms by which transitions between flow patterns will take place, before predicting the conditions under which transition occurs. The task of constructing flow transition boundary curves or maps is usually straightforward, but there is considerable disagreement among authors as to the mechanism for these transitions, and that is reflected in the equations. A good equation of

TABLE 2.1: Flow regime transitions approaches

Type of correlation	Description	References
Empirical	The transition velocity is an empirical equation	Wilkinson and v. Dierendonck [21], Reilly et al. [22]
Semi-empirical	The physical mechanisms are combined with the experimental observations	Taitel et al. [17], Mishima and Ishii [10]
Stability theory	The two-fluid model is used to study the stability of a flow. Developed to model regime transition in bubble columns.	Lissester and Fowler (1992), Joshi et al. (2001)
CFD	The two-fluid model with k-ϵ turbulence in Eulerian framework is used for theoretical prediction of flow regime transition with population balance model (PBM)	Wang et al. (2005)

transition can be expected to apply generally without the need for scale-up rules or procedures. The influence of fluid properties and pipe size as well as flow rates must be accounted.

2.3.1 Bubbly to Slug transition

When gas is introduced at low flow rates (low superficial velocity) into a large diameter vertical column of liquid, the gas phase is distributed into discrete bubbles. Bubbly flow is characterized by an array of smaller bubbles moving in zig-zag motion.

The transition from the condition of bubbly flow to slug flow requires a process of agglomeration or coalescence. In small pipes ,the discrete bubbles combine into a larger vapor slug, having a diameter nearly that of the tube, with lengths of one or two diameters. In large pipes there aren't this condition and the slug bubbles doesn't appear. As the gas flow rate increases, the bubble density increases and the closer bubble spacing results in an increase in the coalescence rate. In this case, the turbulent fluctuations associated with the flow can cause breakup of larger bubbles just formed.

If this breakup is sufficiently intense to prevent re-coalescence, the dispersed bubble pattern can be maintained.

To predict conditions for this transition, it must determined each factors that dominate the process. The dynamics of bubble motion demonstrate that if the bubbles are very small, they behave as rigid spheres rising vertically in rectilinear motion. Above a critical size (about 1.5 mm for air/water at low pressure) the bubbles begin to deform, and the upward motion is a zig-zag path with considerable randomness. The bubbles randomly collide and coalesce, forming a number of somewhat larger individual bubbles with a spherical cap similar to the Taylor bubbles of slug flow, but with diameters smaller than the pipe [10]. The Taylor bubbles are not large enough to occupy the cross section of the pipe so as to cause slug flow. With increases in gas flow rate (at low liquid rates) the bubble density increases and the transition to slug is reached where the dispersed bubbles become so closely packed and the rate of agglomeration to larger bubbles increases sharply.

Mishima and Ishii [10] give a semi-theoretical approach to the problem to determine the boundary between the regimes, by considering a tetrahedral structure in which the individual bubble fluctuates, with a sphere of influence around each bubble. These spheres of influence can overlap in certain situations and the summation of the sphere volume equals the total volume of gas-liquid dispersion. The number of collisions and coalescence is considered to become very large if the maximum possible gap between two bubbles becomes less than a bubble diameter $2r_b$ (see Fig. 2.3). This condition requires that:

$$\alpha|_{bts} = \left(\frac{2}{3}\right)^3 \approx 0.3 \tag{2.2}$$

Griffith and Snyder [23] found that the void fraction at which this transition happens is between 0.25 and 0.30.

Taitel et al. [17] proposed a transition criteria based on the relations between the superficial volumetric fluxes and the rise velocity of relatively large bubbles. When j_g and j_f are the superficial volumetric fluxes of gas and liquid, respectively, and v_0 is the rise velocity of a large bubble.
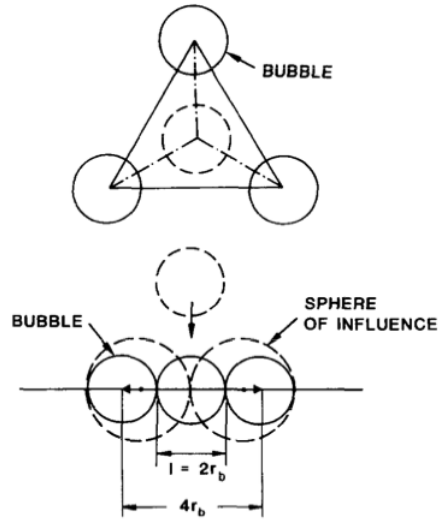
FIGURE 2.3: Bubble packing and coalescence pattern [10]

$$\begin{cases} j_g = \alpha v_g \\ j_f = (1 - \alpha)v_f \\ v_0 = v_g - v_f \end{cases} \tag{2.3}$$

It must necessary to employ a relationship between physical proprieties, of liquid and gas, and the rise velocity. Taitel use a correlation that is insensitive to the bubble size.

$$v_0 = 1.53 \left(\frac{g \Delta \rho \sigma}{\rho_f^2} \right)^{1/4} \tag{2.4}$$

Using Eqs. (2.3) and the condition to the gas holdup to transition $(\alpha_{bts} = 0.25)$ we reach the last formulation of bubbly to slug transition.

$$j_f = 3.0 j_g - 1.15 \left(\frac{g \Delta \rho \sigma}{\rho_f^2} \right)^{1/4} \tag{2.5}$$

Once fluid properties are designated, the theoretical transition curve will remain invariant with the pipe size.

At higher gas and liquid flow rates, where the bubble rise velocity relative to the liquid velocity is negligible, the theoretical transition curve is linear. Vice versa, at low liquid rates where liquid velocity is negligible, the boundary of the bubble region is controlled by the free rise velocity of the bubbles and is essentially independent of liquid rate.

Mishima and Ishii [10] proposed a transition criteria based on a drift-flux reported in Ishii's work [4].

$$\frac{j_g}{\alpha} = C_0 j + \sqrt{2} \left(\frac{\sigma g \Delta \rho}{\rho_f^2} \right)^{\frac{1}{4}} (1 - \alpha)^{1.75} \tag{2.6}$$

where C_0 is given by:

$$\begin{cases} C_0 = 1.2 - 0.2 \sqrt{\dfrac{\rho_g}{\rho_f}} & \text{for round pipes} \\[4mm] C_0 = 1.35 - 0.35 \sqrt{\dfrac{\rho_g}{\rho_f}} & \text{for rectangular pipes} \end{cases} \tag{2.7}$$

The transition from bubbly to slug become:

$$j_f|_{bts} = \left(\frac{3.33}{C_0} - 1 \right) j_g - \frac{0.76}{C_0} \left(\frac{\sigma g \Delta \rho}{\rho_f^2} \right)^{\frac{1}{4}} \tag{2.8}$$

Again, once fluid properties are designated, the theoretical transition curve will remain invariant with the pipe size and the considerations are the same of Taitel's criteria.

In the special case of tubes of small diameter a different transition mechanism occurs. Consider zone I of Fig. 2.2, the rise velocity of the large bubbles relative to the liquid is given by Eq. (2.4) and depends only on the properties of the fluids. The rise velocity of the Taylor bubbles relative to the mean velocity of the liquid is property independent [17].

$$u_g = 0.35 \sqrt{g D_h} \tag{2.9}$$

When $v_0 > u_g$, the rising bubbles approach the back of the Taylor bubble and coalescing with it. Under these conditions bubbly flow cannot exist in zone I. When $v_0 < u_g$, the Taylor bubble rises through the array of distributed bubbles and the relative motion of the liquid at the nose of the Taylor bubble sweeps the small bubbles around the larger one, and coalescence does not take place.

For air/water systems at low pressure, $v_0 = u_g$ and $D_h = 5.0$ cm. For tubes smaller than this value, no bubbly flow can exist below the curve B and the entire zone I and III exist as the slug flow pattern.

Only at high liquid rates (zone II) bubbly flow exist for small tubes where dispersion occurs due to turbulence. A system having a small diameter is one which satisfies the criterion below.

$$\left(\frac{\rho_f^2 g D_h^2}{\sigma \Delta \rho} \right)^{1/4} \leq 4.36 \tag{2.10}$$

Regardless of how much turbulent energy is available to disperse the mixture, bubbly flow cannot exist above void fraction of 0.52. Thus, the B curve delimiting dispersed bubbly flow must terminate at the curve C.

2.3.2 Slug to Churn transition

The slug flow pattern is a consequence of an increasing in gas flow rate that it forces the bubbles to become closely packed and coalesce, starting from a bubbly flow pattern. In the case of small pipes, if the process of coalescence continues, the Taylor bubbles are formed, occupy most of the pipe cross sectional area and are axially separated by a liquid slug in which small bubbles are dispersed. The liquid confined between the bubble and the pipe wall flows around the bubble as a falling film (see Fig. 2.4).

There is considerable difficulty in accurately identifying the slug/churn transition because there are different point of view to describe the churn flow itself. Some investigators identify churn flow on the basis of the froth that appears within the gas region, others associate it with the instability of the liquid film adjacent to the Taylor bubble. Taitel et al. [17] characterize the churn flow pattern as that condition where oscillatory
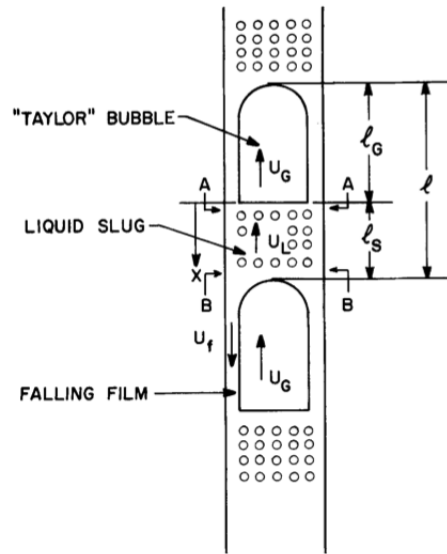
FIGURE 2.4: Slug flow geometry [17]

motion of the liquid is observed. In slug flow, the liquid between two Taylor bubbles moves at a constant velocity and its front as well as its tail have constant speed.

$$v_g = 1.2v_f + 0.35\sqrt{gD_h} \tag{2.11}$$

In this equation the second term on the R.H.S. describes the rise velocity of a large bubble in stagnant liquid and the first term adds the liquid velocity at the centerline, since 1.2 is approximately the ratio of centerline to average velocity in fully developed turbulent flow.

In churn flow, the liquid slug is too short to support a stable liquid bridge between two consecutive slug bubbles. The falling film around the bubble penetrates deeply into the liquid slug and it create a highly turbulent mixture at which point the liquid slug is seen to disintegrate and to fall in a rather chaotic fashion. The liquid re-accumulates at a lower level and the next slug, where liquid continuity is restored, resumes its upward motion. This oscillatory motion of the liquid is considered characteristic to identification of churn flow. There are several mechanisms proposed for transition to the churn pattern:

1. The gas velocity relative to the falling liquid film around the Taylor bubble is approaching to the flooding condition;

2. The Helmholtz instability of the liquid film bounding the Taylor bubble;

3. The individual Taylor bubbles becomes very long;

4. The development length of the condition near the entry region of the pipe.

When the flow pattern is stable *slug flow*, the condition near the entry appears to be churning. The distance that such churning can be observed, before stable slug flow takes place, depends on the flow rates and pipe size. Between the inlet and the position at which at stable slug is formed, the liquid slug alternately rises and falls, and this is the condition of churn flow described by Taitel et al. [17].

As the gas rate increases, it is evident that the length of this entrance region increases and it can occupy the entire length of the test section. It be useful to estimates the lengths over which churn flow is the predominant mode. Taitel develop a method for calculating the entry length required to develop stable slug flow. The distance from the entrance to that length will be observed to be the churn flow pattern.

Suppose that we are in a developed slug flow ($\alpha = 0.25$) and refer to Fig. 2.4. The Taylor bubbles rise at a velocity u_g showed in Eq. (2.11), and the liquid between the Taylor bubbles moves upwards with a velocity u_l. The liquid film adjacent to the bubble flows downward as a free-falling film with velocity u_f. If the liquid slugs are shorter in the developing region (typical churn condition), the velocity distribution in the liquid can be severely distorted by the flow reversal near the wall as a result of the falling film. At the back of the Taylor bubble flow is downward near the wall as a result of the falling film. In order to maintain mass continuity, the velocity at the centerline must increase. Since the velocity of a Taylor bubble depends on the centerline velocity, it is clear that for liquid slugs too short to reestablish the turbulent velocity distribution, the second bubble will overtake the first. As a result, the two bubbles will coalesce, the liquid bridge between them will disintegrate, and fall to a lower level creating churn flow. Designate l_E as the entry length of pipe required to establish stable slug flow and therefore the region that one would observe churning. After many passages we can link the entry length with the diameter and superficial velocity.

$$\frac{l_E}{D_h} = 40.6 \left(\frac{j}{\sqrt{gD_h}} + 0.22 \right) \tag{2.12}$$

The transition postulated by Mishima and Ishii [10] to occur when the mean void fraction over the entire region exceeds that over the slug-bubble section. As described by Taitel, near the conditions of transition, the liquid slugs become unstable to sustain its individual identity due to the strong wake effect generated by neighbor slug bubbles. The mean void fraction over the slug-bubble section (α_m), is obtained by a potential flow analysis applied to the film flow along the bubble until the film flow reaches the void fraction corresponding to the fully developed flow.

The application of the Bernoulli equation yields the local void fraction at the nose of the bubble. The slug-bubble velocity derive form Ishii's work [4] and it's in a drift-flux formulation.

$$v_g = C_0 j + 0.35 \sqrt{\frac{g\Delta\rho D_h}{\rho_f}} \tag{2.13}$$

The mean void fraction is calculated by an integration of nose void fraction over the mean slug-bubble length, and after approximation, have the following expression.

$$\alpha_m = 1 - 0.813 \left\{ \sqrt{\frac{\rho_f}{2g\Delta\rho L_b}} \left[(C_0 - 1)j + 0.35 \sqrt{\frac{g\Delta\rho D_h}{\rho_f}} \right] \right\}^{0.75} \tag{2.14}$$

The mean slug-bubble length at the transition from the slug to churn flow regime may be estimated by the force balance on the liquid film around the slug bubble. In a explicit form, after many passage, the solution for the slug-bubble length becomes. The length depends on the development of the slug flow (injection, entry length, etc.). Since it is assumed that the transition from the slug to churn flow regime occurs when the mean void fraction over the entire region reaches the mean void fraction in the slug-bubble section, the transition criterion becomes.

$$\frac{jg}{C_0 j + 0.35\sqrt{\frac{gD_h\Delta\rho}{\rho_f}}} = 1 - 0.813 \left[\frac{(C_0 - 1)j + 0.35\sqrt{\frac{gD_h\Delta\rho}{\rho_f}}}{j + 0.75\sqrt{\frac{gD_h\Delta\rho}{\rho_f}}\left(\frac{\Delta\rho g D_h^3}{\rho_f \nu_f^2}\right)^{1/18}} \right]^{0.75} \quad (2.15)$$

2.3.3 Transition to Annular flow

For very high gas flow rates the flow becomes annular: the liquid film flows upwards adjacent to the wall, and gas flows in the center carrying entrained liquid droplets. The upward flow of the liquid film against gravity results from the forces make by the fast moving gas core. This film has a wavy interface and tend to break and enter into the gas core as entrained droplets.

Taitel et al. [17] suggest that annular flow cannot exist, unless the gas velocity in the gas core is sufficient to lift the entrained droplets. When the gas rate is insufficient, the droplets fall back, accumulate, form a bridge and churn or slug flow takes place. The minimum gas velocity required to suspend a drop is determined from the balance between the gravity and drag forces acting on the drop and the drop size is determined by the balance between the impact force of the gas that tends to break the drop and surface tension forces that hold the drop together. These equations will predict the minimum value below which stable annular flow will not exist. The true gas velocity can be replaced by the superficial volumetric flux of gas phase and the final transition boundary is given.

$$j_g|_{cta} = 3.1 \left(\frac{g\sigma\Delta\rho}{\rho_g^2}\right)^{1/4} \quad (2.16)$$

This transition criteria shows the transition to the annular pattern is independent of liquid flow rate and pipe diameter. For air/water system at ambient conditions, the calculated velocity is about 15 m/s, and the transition boundary is plotted as a vertical line (in a j_g/j_f plot).

Chapter 3

EXPERIMENTAL FACILITY

3.1 Purpose of the experimental facility

The aim of the facility, built in the laboratory of Politecnico di Milano, is the study of a large pipe system, representative of a direct contact chemical reactor, operating at ambient pressure. The final target of this system is a downhole purification of natural gas. Moreover, it may be able to provide detailed information on the flow phenomena and the experimental data can be used to validate numerical models and information on interface area. In fact, literature review points out that flow phenomena in large pipes and small pipes are very different and up to nowadays there are very few works focused on large diameter pipe; moreover, these works are related to co-current two phase flow.

In the present facility, two internal pipes are present and are representative of the final application of the system under study. The objectives of the experimental facility is to provides global and local data about the flow characteristics and structure, in order to develop and calibrate lumped parameter and 3D numerical models for this specific geometrical configuration.

3.2   Experimental setup

The test facility, built using Polymethyl methacrylate (PMMA), has a section based real downhole geometry with a diameter of 240.2 mm, height of 5 m and two internal pipes in order to schematize a possible real system layout. The design of the experimental facility is divided into three parts: the external structure, the test section and the hydraulic system. For the study of flow phenomena occurring in a counter-current two-phase flow, the pipe should be divided in five sections, from the top to the bottom of the vertical pipe, respectively:

1. upper liquid inlet and gas return section;

2. upper developing section just below liquid inlet;

3. test section;

4. lower developing section just above gas inlet;

5. lower liquid return section and gas inlet.

3.2.1   Design of external structure

The external structure has a J-shape section plan with a size of 3.5×3.5 m and a height of about 6 m. It has two floors that allow access to the different parts of the pipe (first floor is at 2.2 m and the second is at 4.4 m). J-section of the structure allows to place the pipe on the center of it.

3.2.2   Design of the test section

The test section is divided in four parts, so that, if there is a problem, such as visual defect, they can be exchanged. Each zone consists of a pipe of 1 m, a measurement area and a visualization section. Pipes and visualization sections are made of transparent PMMA in order to better visualize flow phenomena. The external diameter is 250 mm. Flanges are used to connect the different sections together.

(a) Test section   (b) Sparger   (c) First floor test section
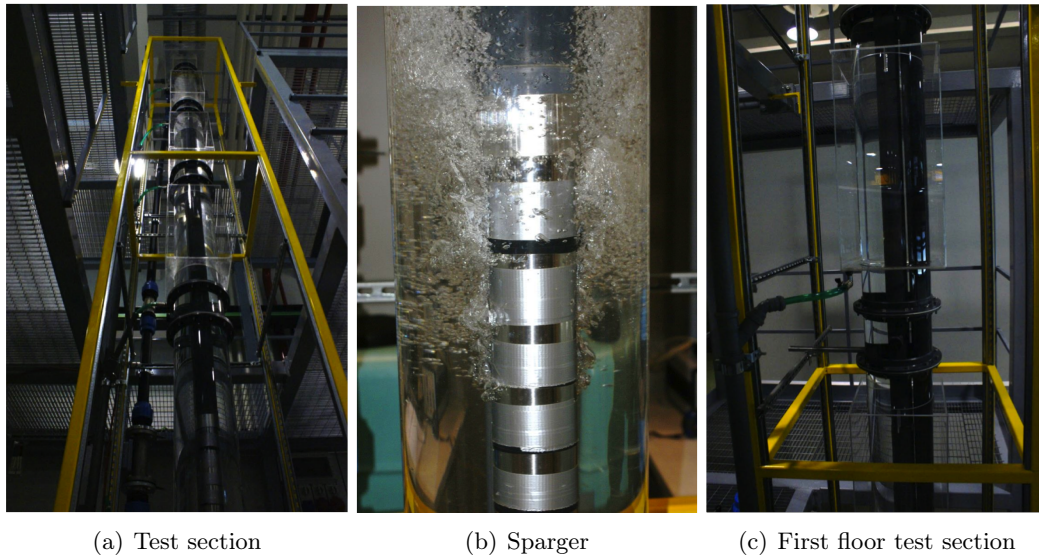
FIGURE 3.1: Local data

To record flow using a video camera it is required a plane surface having a refractive index close to that of the pipe, in order to have the minimum visual deformation. For this reason a viewing area having a square shape also made of PMMA is needed: once this box is filled with a liquid, a relatively close refractive index between the different parts will be obtained. The measurement sections are provided with probe holding on the flanges parts.

At the top of the column there is a reservoir which stores water that will flow in the pipe and the gas that has crossed the whole test section. In fact, in this section of the pipe there is a zone which can both feed the tube with water and let the gas escape inside the tank. The reservoir is connected to three pipes: one of them is used to supply water in order to keep a constant level in the tank; the two other pipes are used to drain if ever there is a surplus of water and to empty the tank if necessary.

3.2.3   Hydraulic and pneumatic systems

The layout of the experimental loop is shown in Figure 3.2. The hydraulic system is divided into two parts: water supply and recovery of water. The main components include two water tanks, a pump, a test section, control and intersection valves. Water is stored in two separator tanks (LTA01, LTA02), open to atmosphere, with volume of,
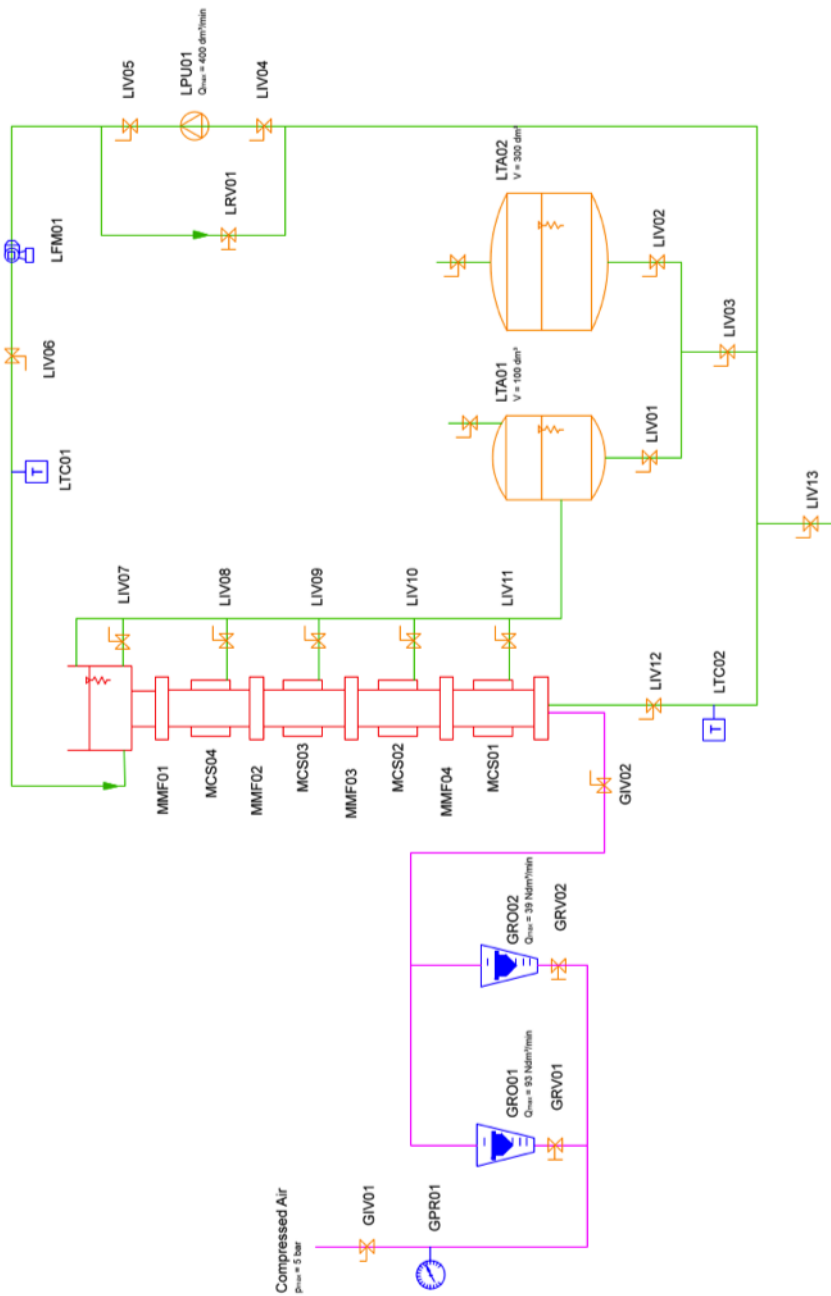
FIGURE 3.2: Test loop

respectively, 100 dm^3 and 300 dm^3. A pump (LPU01) circulates water with a maximum liquid flow rate of 400 m^3 s^{-1} at 2690 rpm. The by-pass valve (LVR01) is used to control the flow rate. At the discharge of the pump, a rotameter (LFM01) measures the water flow rate (from 26.7 dm^3 min^{-1} to 267 dm^3 min^{-1}) and a thermocouple (LTC01) its temperature. The water is sent to the reservoir at the top of the column and then it flows through the pipe. At the outlet of the test section a thermocouple (LTC02) measures the temperature; then water is recirculated by the pump.

Compressed air is supplied from an compressed air line. The pressure is controlled by a regulator (GPR01). Air flow is measured by two rotameters with accuracies of ±2 % f.s.v.: GRO01 measures from 9 dm^3 min^{-1} to 93 dm^3 min^{-1} N.C., GRO02 measures from 40 dm^3 min^{-1} to 240 dm^3 min^{-1} N.C.; the flow rate is adjusted by two valves upstream the rotameters: GRV01 and GRV02. To avoid the reflux of water in the gas line, there is an interception valve (GIV02) upstream the air injector.

The air is injected into a stainless steel tube, 70 mm diameter, 340 mm long, with 180 holes of different diameter (from 2 m to 5 mm). The tube is divided in five strings; in each one there are six rows of holes; every string has the same structure, but staggered, compared to the previous one.

3.3   Experimental technique used

3.3.1   Mass flow rate

A rotameter is a device that measures the flow rate of liquid or gas in a closed tube. It belongs to a class of meters called variable area meters, which measure flow rate by allowing the cross-sectional area the fluid travels through to vary, causing some measurable effect. A rotameter consists of a tapered tube, typically made of glass with a float, actually a shaped weight, inside that is pushed up by the drag force of the flow and pulled down by gravity. Drag force for a given fluid and float cross section is a function of flow speed squared only. A higher volumetric flow rate through a given area increases flow speed and drag force, so the float will be pushed upwards. However, as the inside of the rotameter is cone shaped, the area around the float through which the medium flows increases, the flow speed and drag force decrease until

TABLE 3.1: Measurement instrumentation (flowmeters)

Component code		LFM01		GRO01		GRO02	
Manufacturer		Asa		Asa		Asa	
Model		G6-3100/39 tube	Metal	E5-2600/H tube	Glass	E5-2600/H tube	Glass
Operating fluid		H_2O		Air		Air	
Flow rate range	(Ndm^3/min)	26.7 to 267		9 to 93		40 to 240	
Scale length	(mm)	80		250		250	
Accuracy		±1.5 % f.s.v.		±2 % f.s.v.		±2 % f.s.v.	
Repeatability		0.5 % f.s.v.		< ±0.25% of actual read value		< ±0.25% of actual read value	
Max pressure	(bar)	16		21		21	
Temperature range	(°C)	−10 to 150		0 to 90		0 to 90	

there is mechanical equilibrium with the float's weight. A list of the instrumentation used for this experiment is reported in table 3.1.

3.3.2 Optical void probe

The two-phase flow measuring equipment is composed by the following three distinct elements:

- The optical probe (equipped with standard optical fiber);

- The opto-electronic unit (integrating the photo-trasducer, the amplifier and the shaping of the signals);

- The acquisition box and processing software.

The advantages offered by the optical probe procedures over other techniques make it a favorite research tool for the structural analysis of flows, because:

1. The light, response times are short and insignificant versus those of the probes operating on the electrical properties of the materials (resistive and capacitive probes);

2. The small dimensions of the sensitive areas, a few microns wide bring the optical probe close to being the perfect phase indicator (see Fig. 3.3(a)).
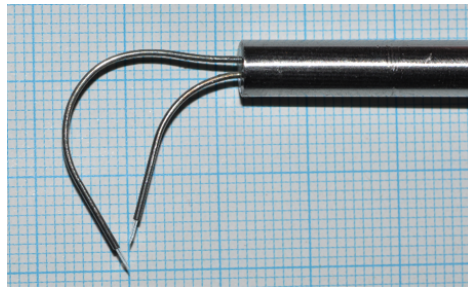
(a) Probe tip
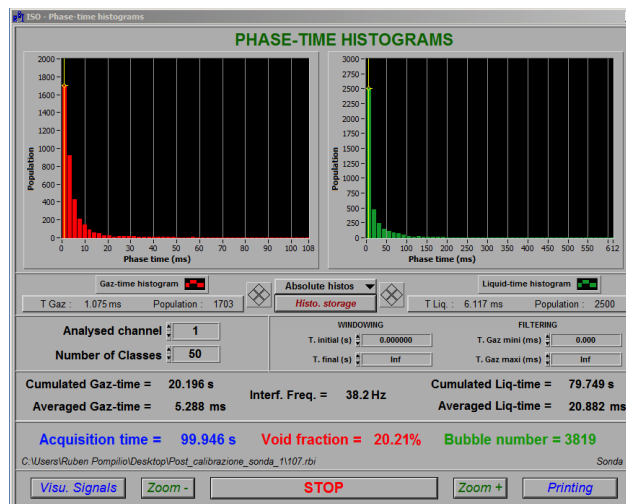
(b) RBI screenshot of phase-time analisys
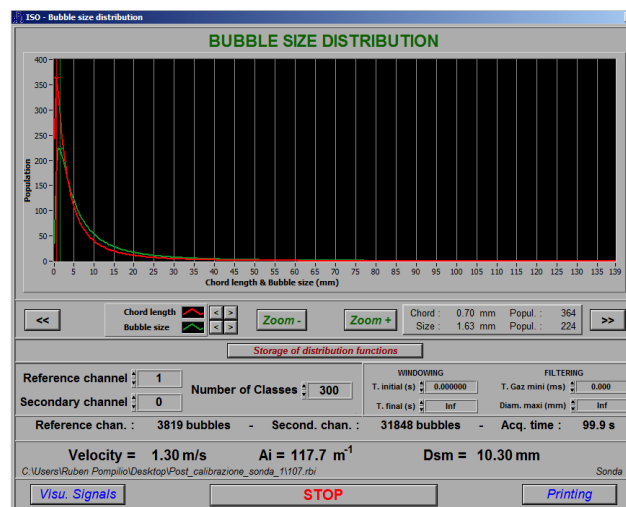
(c) RBI screenshot of bubble size analisys

FIGURE 3.3: Optical void probe instrumentation

When a bubble goes through the optical probe, produces a variable level analog signal to the opto-electronics unit. To be acquired, the signal needs to be shaped. In the RBI-instrumentation[1] acquisition channel, this shaping function is ensured by the acquisition unit. By an automatic thresholding method operation, this module transforms the analog signal obtained through optoelectronic transformation then amplification, into a digital signal. At the conclusion of the acquisition process the results, transferred to the hard disk, consists in a set of records representing the chronological incoming sequence of the leading edges. Each record contains information about the channel concerned, the type of events detected (rising or falling leading edge), the date of the event.

The RBI software (Figs. 3.3(b), 3.3(c)) is a very simple software for post-processing of the digital signal. It produce the data which can be exported even if a channel was filtered due to presence of a disturbing signal (noise). The optical probes are delicate instruments; the calibration must be done very carefully. An oscilloscope can support this step by the increase the accuracy of calibration. The system have high sensibility to interference. Following the procedures of the manufacturer, we proceed to the development of measuring instruments:

1. Measuring the distance between the tips via photo on graph paper: essential to get the speed of the interface from the raw signal;

2. Manual calibration of the optoelectronics unit in the air and water;

3. Setting up acquisition parameters through the GUI of the software: the acquisition time, the maximum number of bubbles and the distance between the tips.

3.4 Data collected

The liquid flow rate is imposed by the water pump and the magnetic flow meter at the outer flange of the pump. So we can ensure a range from $110 \, \mathrm{L\,min^{-1}}$ to $267 \, \mathrm{L\,min^{-1}}$. The gas flow range is imposed by the rotameters and it's a function of the down-well's pressure. From a previous calculus about the conditions of the natural gas inside the

---

[1]The optical void probe manufacture company

well, we have the link between the gas density and the pressure (we have considered five pressure condition of the downhole). The range of air mass flow that we can ensure is from $1389\,\mathrm{L\,min^{-1}}$ to $40\,278\,\mathrm{L\,min^{-1}}$.

We have equally subdivided the entire flow mass range into 13 steps for air and 10 steps for water, then we have 130 conditions to measure. The first step is to evaluate the void fraction with global parameters, for general purpose and, later, check the results from optical void probes.

3.4.1 Global parameters data

This section reports the global void fraction data, calculated from the global volume of gas in the test section. The basic principle of this operation is to collect a large amount of data (for all flow condition) in the easiest way. The default condition is taken only when the water is present in the test section, so the heigh of water level is 3.10 m (from the bottom of the test section) and the volume of water is 0.1155 m^3. From this condition, the global void fraction is calculated at every step of air insufflated in the test section, simply, by calculate the volume correspond to final level of the mixture and subtract from the default volume. The void fraction is calculated by dividing the volume of air and the total volume of the mixture. Data were collected at different levels of pressure: 3 bar, 4 bar and 5 bar and the results are listed in Table 3.2. The measurements are affected by operator error and the fluctuation the water surface caused by gas bubbling. From the visual observation, we note that at low gas flow (80 NL/min), the motion field is complicated and appear structures gaseous form and dimensions are highly variable. Many of these structures that transit internally are not visible nor identifiable.

In general, from visual observation (Fig. 1.2), the bubbles are distorted and has not a regular spherical shape and the shape not to depend upon flow conditions. At high gas flow rate the coalescence of bubble causes periodic recirculation, but the conditions of flooding are never reached.

Obviously, the void fraction increase with the increasing of gas velocity. The void fraction data is slightly influenced by the pressure, in particular increase with the increasing of pressure, due to the higher mass flow rate. The curve (Fig. 3.4) appears

TABLE 3.2: Void fraction data for bubble column mode

| Air flow rate (L min^{-1}) N.C.	j_g (m s^{-1})	Void fraction			
		at 3 bar %	at 3 bar (2) %	at 4 bar %	at 5 bar %
10	0.003	1.4	1.7	0.6	1.6
15	0.004	2.1	-	-	2.2
20	0.005	2.5	3	2.5	3.1
25	0.007	3.4	-	-	3.9
30	0.008	4.5	4.3	4.9	4.6
35	0.009	5.2	-	-	5.5
40	0.01	5.8	6.1	6.1	6.3
45	0.012	6.6	-	-	6.9
50	0.013	7.2	7.3	7.2	7.5
55	0.014	8	-	-	8
60	0.016	8.6	8.8	8	8.8
65	0.017	9.1	-	-	9.4
70	0.018	9.9	10.2	8.8	9.6
75	0.02	10.1	-	-	10.5
80	0.021	10.7	10.8	10.4	11
85	0.022	11.2	-	-	11.2
90	0.023	11.7	11.9	11.9	11.7
95	0.025	12.2	-	-	11.9
100	0.026	12.2	12.9	12.9	12.6
105	0.027	12.4	-	-	12.4
110	0.029	13	13.4	13.6	13.2
115	0.03	13.2	-	-	-
120	0.031	13.5	14.7	13.9	-
125	0.033	14	-	14.4	-
130	0.034	14.6	15.5	15.8	-
135	0.035	-	-	-	-
140	0.036	3.47	16.4	-	-
150	0.039	3.5	17.1	-	-
160	0.042	3.54	18.1	-	-
170	0.044	3.58	19	-	-
180	0.047	3.57	18.8	-	-
190	0.049	3.6	19.4	-	-
200	0.052	3.64	20.3	-	-
210	0.055	3.66	20.8	-	-
220	0.057	3.67	21	-	-
230	0.06	3.71	21.8	-	-
240	0.062	3.75	22.7	-	-
250	0.065	3.78	23.3	-	-
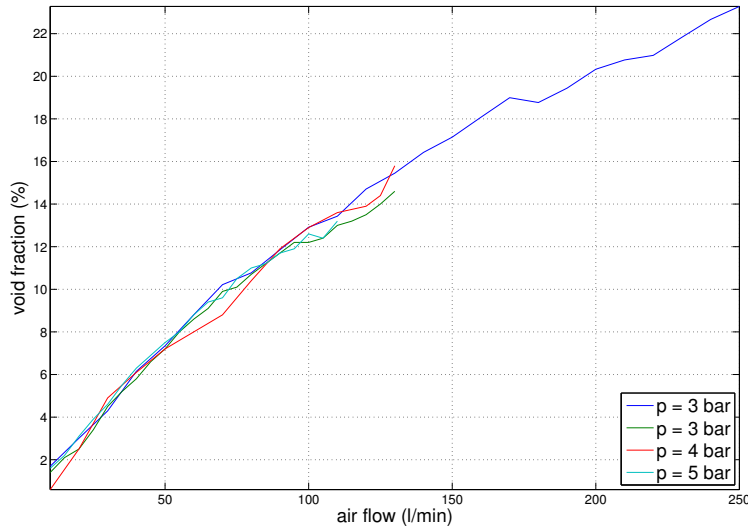
FIGURE 3.4: Bubble column mode data

to have a decreased slope value from 10% to 15% of void fraction: this is a region of transition from bubbly flow to churn bubbly. The data collected in counter-current mode (Fig. 3.5(a)) validate the above consideration about the transition boundary; it is evident the effect of the liquid flow on the slope of the void fraction curve; this is more accentuate at higher liquid fluxes. With a liquid flow in downward direction, we can see the effect of liquid flow rate of void fraction: at fixed gas velocity, if the liquid velocity increases, the void fraction increases due to the bubbles dispersion in the radial direction.

Comparing the models in the literature and the database of the global void fraction, is possible to observe that the models underestimate of two orders of magnitude the void fraction at very low mixture superficial velocity. The main reason is because these models have been developed for operating conditions that correspond to high flow rates present in the vessel of nuclear reactors; this leads to an incorrect calculation in low speed conditions. Hence, it is necessary to use specific models or a set of models that combined together can overcome this issue.
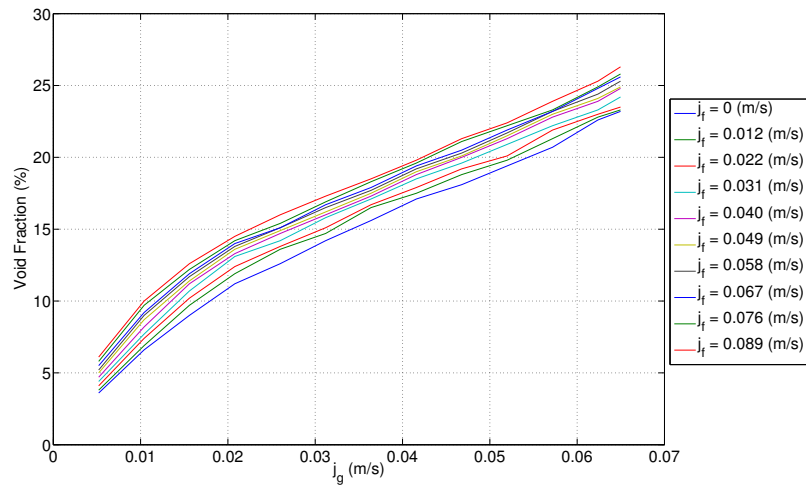
(a) Global data
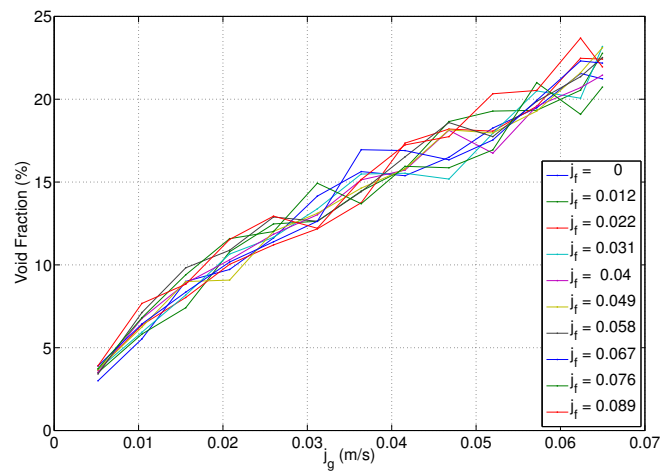
(b) Local data

FIGURE 3.5: Countercurrent data

3.4.2 Optical void probe data

The next step was to validate the void fraction measurements taken with the optical probes and pick up a new database based on local void fractions near the gas distributor, to see if the flow is fully developed. The collected data include: the size distribution of bubble, useful for the initial conditions of the CFD software to calculate correctly the drag law; interfacial area and frequencies, the number of bubbles and their velocity

(with the cross-correlation mode). The optical probe is inserted at a height of 2 m from the gas sparger, so that the flow is sufficiently developed and at the same time not affected by the boundary condition of the water surface with falling water.

It is noted that the channel corresponding to the tip more upstream with respect to the direction of gas flow records a number of bubbles of an order of magnitude higher than that of the other channel. This is because most of the detected bubbles are of the order of 0.1 mm. Bubbles so small are not of interest compared to the analysis of the motion field that you want to perform, and then arises for this channel a filter of 0.1 ms on the minimum time of crossing of the bubbles and in this way the number of returns to be the same order of magnitude as that of the parallel channel. The fact that a channel counts many bubbles of small diameter does not affect the calculation of the void fraction, unlike the sauter mean diameter calculation.
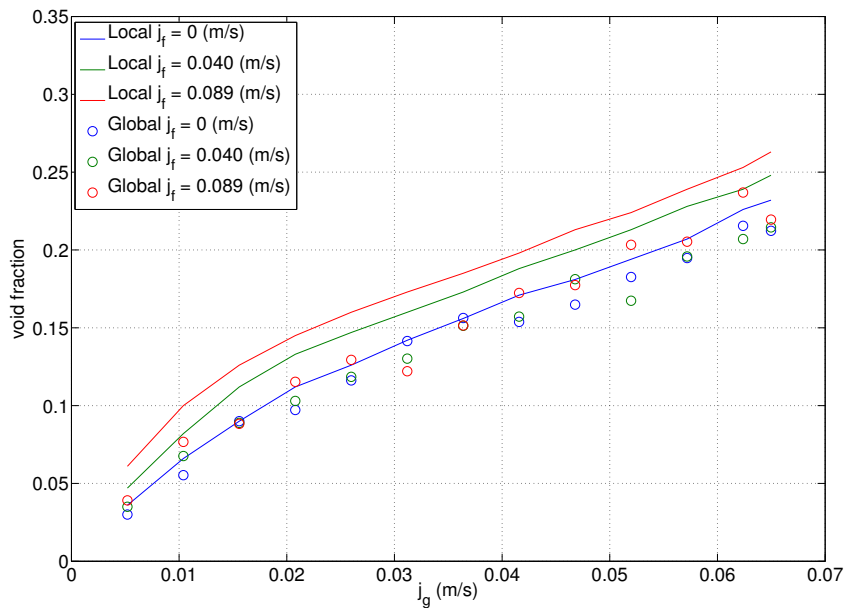
FIGURE 3.6: Comparison between global data and local data from optical probe

From Fig. 3.6 there is a correspondence in the void fraction trend, but a difference between the measured values with the global method and those obtained by the optical probes. This phenomenon could be due to the fact that the calculation of the void fraction with the global procedure gives an average value over the entire column. In

reality there is a void fraction gradient along the column, causing a deviation between the trend of the global value and the measured locally by the probe at a certain height.

Here are reported the data collected with the optical probes. It may be noted that the void fraction is more scattered at high gas flow, due to the increased turbulence of the flow in the pipe (Fig. 3.5(b)). To reduce this effect should increase the integration time of the signal acquisition. The bubble size distribution seems to increase with the increasing of liquid superficial velocity because the drag force of bubbles increase and decrease their velocity, additional, their tend to occupy entire section, with an increasing of coalescence. The bubbles number natural increases due to increase the gas velocity. *The interfacial area per unit volume of two-phase flow* is a useful parameter for observing a transitional boundary. The rising velocity is a useful parameter to check the cross correlation algorithm of the optical probe and it's correlated to the buoyancy with the superficial tension and the kinematic viscosity.

The acquisitions through optical probe confirms the usefulness of the probe in all conditions of interest. However, they exhibit large discrepancies in the number of bubbles from the two probe tips, due to the instability of the contact between the optical fiber and the optoelectronic unit (Fig. 3.7). The difference in the number of bubbles recorded affect the sensitive element of the probe. It might be a problem with fluid due to interfacial phenomena or trend of the flow with respect to the tips. The effects of the bubbles number are negligible and it can be filtered during post-processing of results.

3.4.3 Bubbles diameter

The optical probes are able to provide data on the population diameters of the bubbles. Therefore, some considerations can be made on the diameter of the bubbles. If the diameter of the bubbles is small, the system will be able to have the mass and energy exchange, fast and efficient. The analysis on the bubbles population, in five different operative points, has determined that the diameters of the bubbles are between 5 and 25 mm. In particular, at minimum gas flow rates, the diameters are 5.30 mm with no liquid flow and 6.43 mm with the maximum liquid flow. The increment of the diameter is 21.14%. At maximum gas flow rates, the diameters are 24.77 mm with no liquid
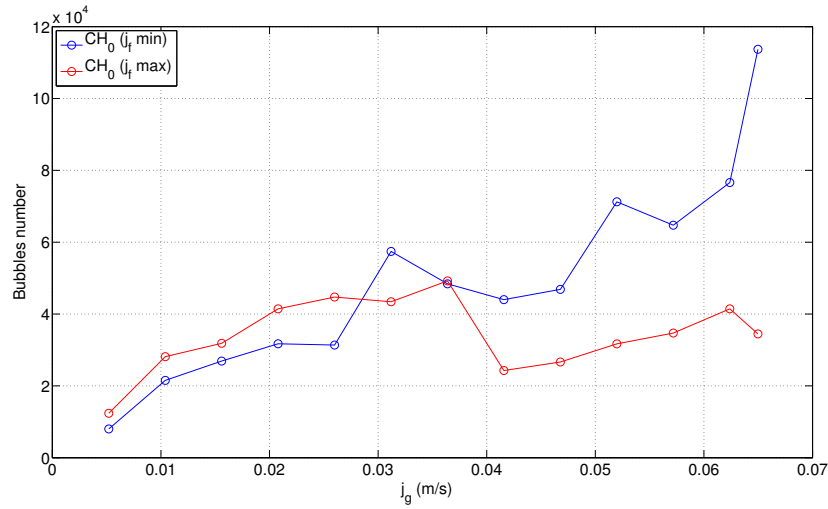
(a) Bubbles number from channel 0 (not filtered)
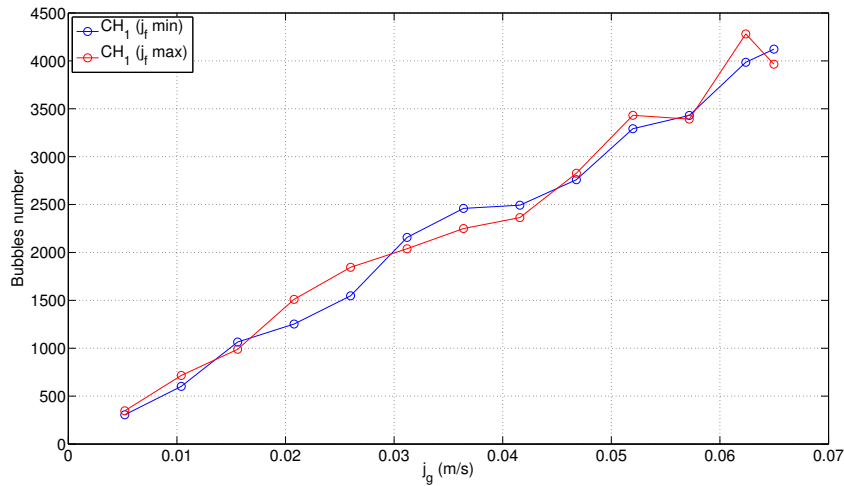
(b) Bubbles number from channel 1

FIGURE 3.7: Bubbles number from optical probes

flow and 22.13 mm with the maximum liquid flow. The increment of the diameter is 10.66%. In the middle operating point (gas flow: $120 \, \mathrm{L\,min^{-1}}$, liquid flow: $90 \, \mathrm{L\,min^{-1}}$) the diameter is 23.36 mm.

Despite the diameter of the bubbles on the walls of the tube is always approximately constant, the large structures of gas that move internally increase the sauter mean diameter and this explains an increase from 2.5 to 3.5 times the diameter under the

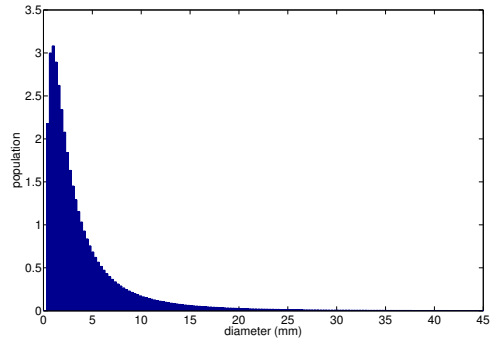conditions of the minimum gas flow.
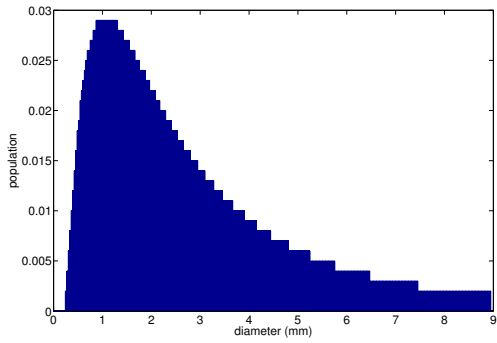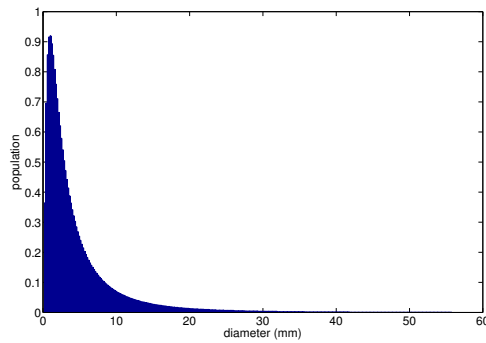

(a) Minimum gas and liquid flow rates
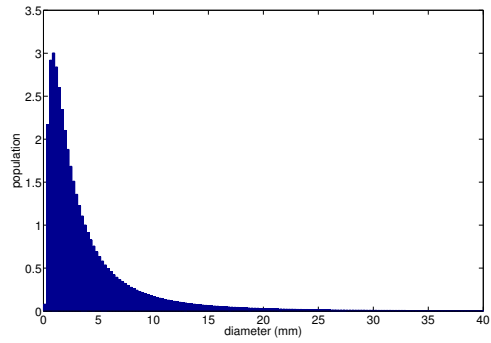
(b) Maximum gas flow rates and minimum liquid flow rates
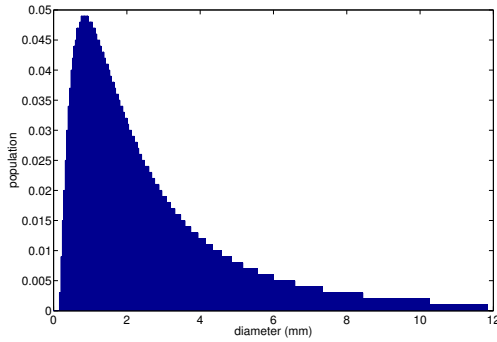
(c) Minimum gas flow rates and maximum liquid flow rates

(d) Maximum gas and liquid flow rates

(e) Middle range of operating points

FIGURE 3.8: Bubbles diameter population distributions

Chapter 4

COMPREHENSIVE DRIFT-FLUX MODEL FOR VERTICAL PIPES

In this thesis, data and models of various researchers have been collected, analyzed and compared to the various drift-flux models available in the literature for large pipes. This comparison was then used to develop a series of models drift-flux for use in pipes of all sizes in all flow conditions. The data were also used to investigate the effects of pipe diameter and axial development on two-phase flow in large pipes.

The importance of a comprehensive drift-flux model is to have a model which can employed in a two-fluid model, as closure model, because the calculation of the interfacial drag requires a constitutive models based on the drift-flux, to compute the area-averaged relative velocity from the void-weighted average gas and liquid velocities from the momentum equation. In particular, the application of this class of model to forced convection systems has been quite successful.

4.1 State-of-the-art for vertical pipes

In general, the mechanism by which the two fluids interact is dictated by the flow regime. Therefore, the correlation used to predict the behavior of the two-phase flow in small pipes will not be applicable to the large ones due to the change of the flow structure. Many scientists have developed relationships in the past and the search field

is projected into the future by looking for new ways to generalize the correlations for a wider range of flow maps and various operating conditions [24]. The trend of modern correlations is to be more specific to the flow regime considered and are often further subdivided on the basis of velocity or diameter to try to be more efficient.

In the literature [24, 12, 4, 8] numerous correlations are available to predict the void fraction in upward two phase flow while comparatively fewer correlations are proposed for downward orientation. In general, the correlations developed for vertical upward flow failed to predict the void fraction for downward orientation but, the correlations based on the concept of the drift flux model could be used to predict the void fraction in both orientations with a slight change in its computational structure. If the sign of the drift term is changed to negative, the correlations based on drift flux model can be applied to both upward and downward orientations.

Much care should be taken in the use of these correlations because, most of these, are developed by different investigators and were based on the data limited in number, pipe diameter, flow pattern, fluid combinations and system pressure. While the literature shows significant attempts to classify flow regimes in large diameter pipes, no comprehensive flow regime transition model has been developed.

4.1.1 Small pipes

4.1.1.1 Mechanistic drift-flux model by Ishii [4]

Ishii [4] is one of the first scientists who have implemented the mechanistic theory of drift-flux model in the 70s specifically designed for small pipes. He developed a comprehensive set of drift-flux models for small circular pipes as well as rectangular channels. These models are often used due to simplicity and accuracy across a wide range of conditions.

For the distribution parameter, Ishii [4] has developed a simple correlation in upward two-phase flow, based on the density ratio of the two fluids and on the Reynolds number, in a fully developed bubbly flow. After a numerous tests with a wide range of Reynolds number, the Eq. (1.20) can be approximated with 1.2 for an upward flow in a round

pipe. For the annular flow regime, he used a more complex formulation derived from the formulation of the drift term and the mean drift velocity:

$$\overline{v_{gj}} \equiv v_{gj} + (C_0 - 1)j \tag{4.1}$$

$$C_0 = 1 + \frac{1 - \alpha}{\alpha + 4\sqrt{\rho_g/\rho_f}} \tag{4.2}$$

Starting from the definition of the Eq. (4.1) and eliminating the pressure gradient from the momentum equation (because the model is designed for steady-state adiabatic flows), introducing the general drift-flux formulation by Zuber and simplify, we obtain the formulation of the drift term for annular flow:

$$v_{gj} = 1 + \frac{1 - \alpha}{\alpha + 4\sqrt{\rho_g/\rho_f}} \sqrt{\frac{gD_h\Delta\rho(1 - \alpha)}{0.015\rho_f}} \tag{4.3}$$

By considerations of drag and lift equilibrium on the bubble system, Ishii has obtained the drift term for the other flow regimes by taking into account the geometry, the body-force field, the shear stresses, and the interfacial momentum transfer.

For *Churn flow*:

$$v_{gj} = \sqrt{2} \left(\frac{\sigma g\Delta\rho}{\rho_f^2} \right)^{0.25} (1 - \alpha)^{0.25} \tag{4.4}$$

For *Slug flow*:

$$v_{gj} = 0.35 \sqrt{\frac{gD_h\Delta\rho}{\rho_f}} \tag{4.5}$$

For *Bubbly flow*:

$$v_{gj} = \sqrt{2} \left(\frac{\sigma g \Delta \rho}{\rho_f^2} \right)^{0.25} (1 - \alpha)^{1.75} \tag{4.6}$$

Ishii [4] also developed an equation for boiling flow: the formulation of the distribution parameter is based on the number of nucleating sites and depends on the void fraction.

$$C_0 = \left(1.2 - 0.2\sqrt{\rho_g/\rho_f} \right) (1 - e^{-18\alpha}) \tag{4.7}$$

The distribution parameter by Ishii [4] can be applicable over a wide range of regimes because, in small pipes, the shape of the bubbles and the liquid film around gas slugs remains similar from one regime to another. Therefore, void fraction and velocity profiles remain similar.

4.1.1.2 Drift-flux model by Hibiki and Ishii [5]

Hibiki and Ishii [5] have obtained the same drift term by Ishii, but a modified distribution parameter which suggests that the dominant factor to determine the distribution parameter in vertical upward bubbly flow would be the bubble sauter mean diameter.

$$\begin{cases} C_0 = \left(1.2 - 0.2\sqrt{\rho_g/\rho_f} \right) (1 - e^{-22d_s/D}) \\ v_{gj} = \sqrt{2} \left(\frac{\sigma g \Delta \rho}{\rho_f^2} \right)^{0.25} (1 - \alpha)^{1.75} \end{cases} \tag{4.8}$$

In the following proposed models, the distribution parameter was taken without the diameter correction.

4.1.2 Intermediate pipes

For Schlegel et al. [24], the transition region between small and large pipes begins at non-dimensional hydraulic diameter of 18.6 and ends at a value of 30. In this region, he recommend a linear interpolation to describe the transition from one regime to another,

even from one diameter to another. Therefore, the drift-flux's parameters changes their structure to include the interpolation (Eq. (4.9)). Λ represent the weighting factor of the physical parameter or flow regime, the subscript A represents the left boundary of the domain and the subscript B represents the right one. Finally, p represent a parameter of the drift-flux model.

$$p_{A,B} = p_A \Lambda + p_B(1 - \Lambda) \tag{4.9}$$

In each flow regime the mechanisms that govern the interactions between the phases are very different, meaning that the correlations must be different. This requires that the flow regimes be mapped and the transitions be accurately predicted.

A further model to describe the transition between flow regimes has been proposed by Hasan et al. [25]. They use an exponential functions to obtain a continuous function over the entire range of transition. They provide a function for the calculation of the distribution parameter which interpolate the transition between the facility configurations (i.e. upward, downward and countercurrent). For example, for the transition between bubbly and slug flow has been proposed by the following equation:

$$C_0 = C_{0,b} \left(1 - e^{-0.1v_{bs}/(j_g - v_{bs})}\right) + C_{0,s} \left(e^{-0.1v_{bs}/(j_g - v_{bs})}\right) \tag{4.10}$$

Where C_0 is the dimensionless distribution parameter, $C_{0,b}$ is the dimensionless parameter for fully developed bubbly flow and $C_{0,s}$ is the dimensionless parameter for fully developed slug flow. v_{bs} is the transition velocity.

In this thesis, we have adopted a similar approach to Hasan, taking advantage of the continuity properties of the exponential function through the use of a probabilistic formulation of the transitions between flow regimes. we have taken the probability density functions (i.e. the Gaussian) for both the transitions between the flow regimes and for both the transition between the diameters (Eq. (4.11)). Where f is the smoothing coefficient and p is the physical parameter. All is described more fully in section 4.2.

$$f = \frac{1}{2} \left[1 + \text{erf}\left(\frac{p}{\sqrt{2}}\right)\right] \tag{4.11}$$

4.1.3   Large pipes

In any channel larger than the size predicted by Eq. (2.1), large Taylor cap bubbles cannot occupy the entire cross-section of the channel without becoming unstable and breaking up. For air-water flows at atmospheric conditions this is about 10 cm. For developing a new drift-flux correlation it must be taken in account three main peculiarity of the large pipes systems, which are reflected into these correlations:

1. the radial profile of void fraction, in large pipes, will be different from those of small pipes in particular is more flat in large pipes;

2. the drift-flux velocity, in large pipes systems, increase due to the reduced influence of the pipe wall;

3. the recirculation patterns due to turbulence can modify the drift-flux parameters, because to the increased diffusion.

4.1.3.1   Drift flux model by Hills [6]

Hill, in 1976, developed following drift-flux type correlations based on his own database with a diameter of 15 cm and height of 10.5 m:

$$
\begin{cases}
v_g = 1.2j + 0.24 & \text{for } j_f > 0.3 \text{ m/s} \\
v_g = j + (0.24 + 4.0\alpha^{1.72})(1 - \alpha) & \text{for } j_f \leq 0.3 \text{ m/s}
\end{cases}
\tag{4.12}
$$

In these correlations, the unit of parameters should be m/s, since the mixture volumetric flux in his experiment should be 6.2 m/s at maximum.

Obviously, this model performs well for Hills database, but it is empirical and therefore may not perform well for conditions outside those seen in his experiments. Additionally, fluid properties are not explicitly taken into account, so the correlation may not work very well for systems other than air-water at atmospheric conditions.

4.1.3.2 Drift flux model by Shipley [7]

Shipley proposed this correlation based on his own database measured in a pipe with an inner diameter of 45.7 m and a height of 5.64 m. This correlation is empirical and fluid properties are not accounted for. Additionally, the inclusion of diameter in the drift velocity term indicates that as diameter increases, the relative velocity will increase up to unrealistic values.

$$v_g = 1.2j + 0.24 + 0.35 \left(\frac{j_g}{j} \right)^2 \sqrt{gD_h\alpha} \tag{4.13}$$

4.1.3.3 Drift-flux model by Clark and Flemmer [8]

Clark and Flemmer, in 1985, developed a semi-empirical correlation based on the measured void fraction in a pipe with a diameter of 10 cm employing air and water as woking fluids. In this experiment, they observed that occasional large cap bubbles were formed. The correlations they proposed was:

$$v_g = 0.934(1 + 1.42\alpha)j + 1.53 \left(\frac{\sigma g}{\rho_f} \right)^{0.25} \tag{4.14}$$

The physical proprieties are implicitly accounted for C_0 by employing the void fraction and are accounted in the drift term with the superficial tension and liquid density. The performance of this model are the same of the Hills one and it can not early be applied to systems, in particular, with steam at high pressure because the gas density are not accounted for.

4.1.3.4 Drift flux model by Kocamustafaogullari and Ishii [9]

Kocamustafaogullari and Ishii [9] developed a semi-empirical correlation for the drift velocity for two-phase flows in large pipes with density ratios and viscosity. This correlations are the drift term and vary with diameter.

$$
\begin{cases}
v_{gj} = 0.54\sqrt{\dfrac{gD_h\Delta\rho}{\rho_f}} & \text{for } D_h^* \leq 30 \\[3ex]
v_{gj} = 3.0\left(\dfrac{\sigma g\Delta\rho}{\rho_f^2}\right)^{0.25} & \text{for } D_h^* > 30
\end{cases}
\tag{4.15}
$$

For a fully developed turbulent flow in a round tube, the distribution parameter is:

$$
C_0 = 1.2 - 0.2\sqrt{\frac{\rho_g}{\rho_f}}
\tag{4.16}
$$

4.1.3.5 Drift flux model by Mishima and Ishii [10]

Mishima and Ishii developed a model for large pipes with the drift-velocity that depend upon diameter, system pressure, gas flux and fluid physical properties. According to their model, the distribution parameter is the same as Ishii [4], $C_0 = 1.2 - 0.2\sqrt{\rho_g/\rho_f}$, and drift velocity is defined as:

$$
\begin{cases}
v_{gj} = 0.0019 D_h^{*\,0.809}\left(\dfrac{\sigma g\Delta\rho}{\rho_f^2}\right)^{0.25}\left(\dfrac{\rho_g}{\rho_f}\right)^{-0.157} N_{\mu f}^{-0.562} \\[3ex]
v_{gj} = 0.030 D_h^{*\,0.809}\left(\dfrac{\sigma g\Delta\rho}{\rho_f^2}\right)^{0.25}\left(\dfrac{\rho_g}{\rho_f}\right)^{-0.157} N_{\mu f}^{-0.562}
\end{cases}
\tag{4.17}
$$

The first equation is for $D_h^* \leq 30$, and the second one for $D_h^* > 30$. Where the viscosity number is defined as:

$$
N_{\mu f} = \frac{\mu_f}{\left(\rho_f\sigma\sqrt{\frac{\sigma}{g\Delta\rho}}\right)^{0.5}}
\tag{4.18}
$$

The above equations are valid for low viscous case ($N_{\mu f} \leq 2.25 \times 10^{-3}$). For the high viscous case the drift term must be used is:

$$
v_{gj} = 0.92\left(\frac{\rho_g}{\rho_f}\right)^{-0.157}
\tag{4.19}
$$

This model was developed and verified for pool conditions, so liquid flow rate of zero, and was verified for forced convection flows by Schlegel et al. [24]. These experiments showed that Kataoka and Ishii's model worked well at moderate void fractions ($\alpha \leq 0.4$).

4.1.3.6 Drift flux model by Kawanishi et al. [11]

In 1990, Kawanichi et al. developed a drift-flux model based on the work done by Ishii [4], but modified the drift velocity for large pipes as:

$$
\begin{cases}
v_{gj} = \dfrac{1}{2}\left[0.52\sqrt{\dfrac{D_h g \Delta\rho}{\rho_f}} + \sqrt{2}\left(\dfrac{\sigma g \Delta\rho}{\rho_f^2}\right)^{0.25}\right] & \text{for } 0 \leq j \leq 0.24 \text{ m s}^{-1} \\[4ex]
v_{gj} = 0.52\sqrt{\dfrac{D_h g \Delta\rho}{\rho_f}} & \text{for } j > 0.24 \text{ m s}^{-1}
\end{cases}
\tag{4.20}
$$

This model attempts to account for the increased drift velocity in large pipes, however, from other experiments by Isao and Mamoru [15], we know that for large pipes the drift velocity is independent of diameter, while this correlation indicates that the drift velocity increases with diameter, which may become physically unrealistic for pipes with very large diameters. Again, this correlation is empirical and is not suitable to predict conditions outside those used in the initial benchmarking data set.

4.1.3.7 Drift flux model by Hibiki and Ishii [12]

Hibiki and Ishii [12] developed correlations applicable to bubbly and cap bubbly flows in large diameter channels with void fractions less than 0.3. They noted that for bubbly flow in large pipes, the drift-flux parameters are dependent on the inlet conditions. If the inlet flow regime is *bubbly flow* with small and uniformly distributed bubbles, the distribution parameter is:

$$\begin{cases} C_0 = \exp\left[0.475\left(\dfrac{j_g}{j}\right)^{1.69}\right]\left(1 - \sqrt{\rho_g/\rho_f}\right) + \sqrt{\rho_g/\rho_f} \\[3mm] C_0 = \left[-2.88\left(\dfrac{j_g}{j}\right) + 4.08\right]\left(1 - \sqrt{\rho_g/\rho_f}\right) + \sqrt{\rho_g/\rho_f} \end{cases} \tag{4.21}$$

The first equation is for $0 \le j_g/j \le 0.9$, and the second one for $0.9 < j_g/j$. The following equations describe the drift term of this model. The first equation is developed by Hibiki and Ishii [5] and the second by Mishima and Ishii [10]:

$$\begin{cases} v_{gj} = \sqrt{2}\left(\dfrac{\sigma g \Delta\rho}{\rho_f^2}\right)^{0.25}(1-\alpha)^{1.75} \\[3mm] v_{gj} = 0.0019\min(D_h^*, 30)\left(\dfrac{\sigma g \Delta\rho}{\rho_f^2}\right)^{0.25}\left(\dfrac{\rho_g}{\rho_f}\right)^{-0.157}N_{\mu f}^{-0.562} \end{cases} \tag{4.22}$$

The merging between these equations are made by a linear interpolation with the exponential as smoothing coefficients:

$$v_{gj} = v_{gj,HI}e^{-1.39j_g} + v_{gj,KI}\left(1 - e^{-1.39j_g}\right) \tag{4.23}$$

When the gas phase is introduced as larger cap bubbles the drift velocity formulation is identical to above one, but the distribution parameter change as:

$$\begin{cases} C_0 = 1.2\exp\left(0.11j_g^{2.22}\right)\left(1 - \sqrt{\rho_g/\rho_f}\right) + \sqrt{\rho_g/\rho_f} \\[3mm] C_0 = 0.6\exp\left(-1.2j_g1.8\right) + 1.2\left(1 - \sqrt{\rho_g/\rho_f}\right) + \sqrt{\rho_g/\rho_f} \end{cases} \tag{4.24}$$

The first equation is for $0 \le j_g \le 1.8$, and the second one for $1.8 < j_g$. This model is valid for void fractions less than 0.3, else, for void fractions above 0.3, is recommended to use the Kataoka and Ishii's model [12].

4.1.4 General considerations about the structure of drift-flux model

A general considerations can be made about the drift-flux for large pipes in literature:

1. model for small pipe cannot be used for large pipes;

2. semi-empirical model have better performance compared with empirical model, due to the presence of physical proprieties in the drift term;

3. in large pipes model should take into account the inlet flow regime conditions.

Many experiments in literature have shown that the effect of diameter on the distribution parameter is negligible as long as the flow is fully developed [15]. Therefore, this effect on the drift-flux correlations must be taken into account in the drift term. When the pipe diameter reaches a dimensionless value of 18.6, the effect of the pipe wall begins to be reduced. At values of dimensionless diameters higher than 30, the pipe is so large that the wall no longer has any effect on the bubble.

Schlegel et al. [24] proposed a comprehensive set of drift-flux models for pipes. That set helps to reduce numerical issues in solving complex equations using computer codes and covers all flow conditions and pipe sizes, but the interpolation criteria is based on a linear interpolation and it should be avoided due to problems with the continuity of the derivates. Therefore, a new set of models is used in this thesis for the model developed in the following sections (Tab. 4.1).

TABLE 4.1: New set of models

Pipe	Flow regime			
	Bubbly	Cap/Slug	Churn	Annular
Small	Hibiki/Ishii [5]	Ishii Slug [4]	Ishii Churn [4]	Hirao
Intermediate	Interpolation	Interpolation	Interpolation	Interpolation
Large	Shipley	Kataoka Slug [10]	Clark + Hirao	Koca/Ishii [9]

4.2 Model conceptual idea

What we want to explain, in this section and in the follower ones, is a comprehensive model that aims to integrate nine different models, developed by various authors between 1960 and 2000, in order to employ an algorithm which calculate the void fraction in a wide range of operative conditions, having as input source: the geometry of the duct (hydraulic diameter and length of the pipe), the thermodynamic properties of the two fluids and the volumetric flow rates. The model takes advantage of interpolator laws of exponential nature, to tie together the different flow regimes and the effect of the diameter. It's been tested with the upward configuration, both for small pipes, pipes for both large and was also compared with the data of counter-current of the Politecnico di Milano, obtaining satisfactory results.

The model bases its calculation on the conditions of transition between different regimes (bubbly, slug, churn and annular), through reports from the literature (briefly described here); subsequently calculates the void fraction throughout the flow field using all models simultaneously. Each void fraction calculated is processed with specific functions interpolator based on Gaussian functions. The models used for the intermediate pipes are the result of a double interpolation between flow regimes and diameters. The coefficients used for the discrimination between the various geometries of the duct (large, intermediate, small), are obtained by exploiting the distribution function of the Gaussian distribution (Eq. (4.25)), where the x assumes the value of the dimensionless diameter, the μ assumes the value of the diameter in transition and σ assumes the value of the standard deviation that best satisfies the values of the database benchmark which is $\sigma = 27.8$ this value is obtained from an average of an array of values computed for every benchmark databases (Tabs. 4.4, 4.6).

$$f = \frac{1}{2}\left[1 + \text{erf}\left(\frac{x-\mu}{\sigma\sqrt{2}}\right)\right] \tag{4.25}$$

The values for the transition are set at $D_{SI}^{+} = 18.6$ for the transition from the small to intermediate pipes, while the transition between intermediate and large pipes was used the value of $D_{IL}^{+} = 30$. The two resulting equations (Eqs. (4.26), (4.27)) are shown in Figure 4.1.
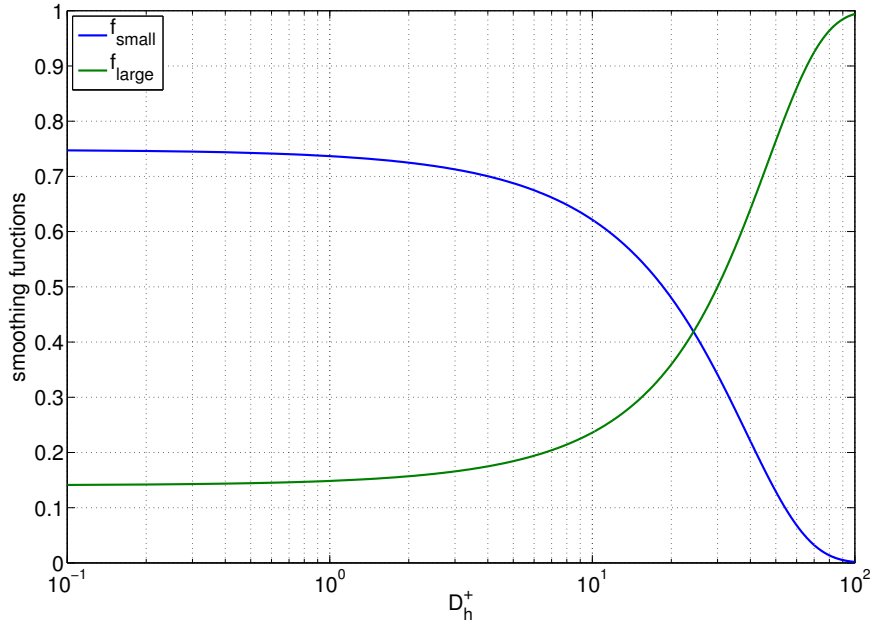
FIGURE 4.1: Diameter coefficients

$$f_{small} = \frac{1}{2}\left[1 + \operatorname{erfc}\left(\frac{D_h^+ - D_{SI}^+}{\sigma\sqrt{2}}\right)\right] \tag{4.26}$$

$$f_{large} = \frac{1}{2}\left[1 + \operatorname{erf}\left(\frac{D_h^+ - D_{IL}^+}{\sigma\sqrt{2}}\right)\right] \tag{4.27}$$

The same procedure was carried out to obtain the formulation of the coefficients for the transitions between the various flow regimes. Functions used here are four, three of which are linearly independent. The values used for transitions refer to equations of the type: $j_{f,trans} = f(j_g)$, already widely described in the previous sections and briefly described here.

$$f_{bubbly} = \frac{1}{2}\operatorname{erfc}\left(\frac{j_g - j_{f,BTS}}{\sigma\sqrt{2}}\right) \tag{4.28}$$

$$f_{slug} = -\frac{1}{2}\operatorname{erfc}\left(\frac{j_g - j_{f,STC}}{\sigma\sqrt{2}}\right) \tag{4.29}$$

(a) Bubbly coefficient

(b) Slug coefficient

(c) Churn coefficient

(d) Annular coefficient
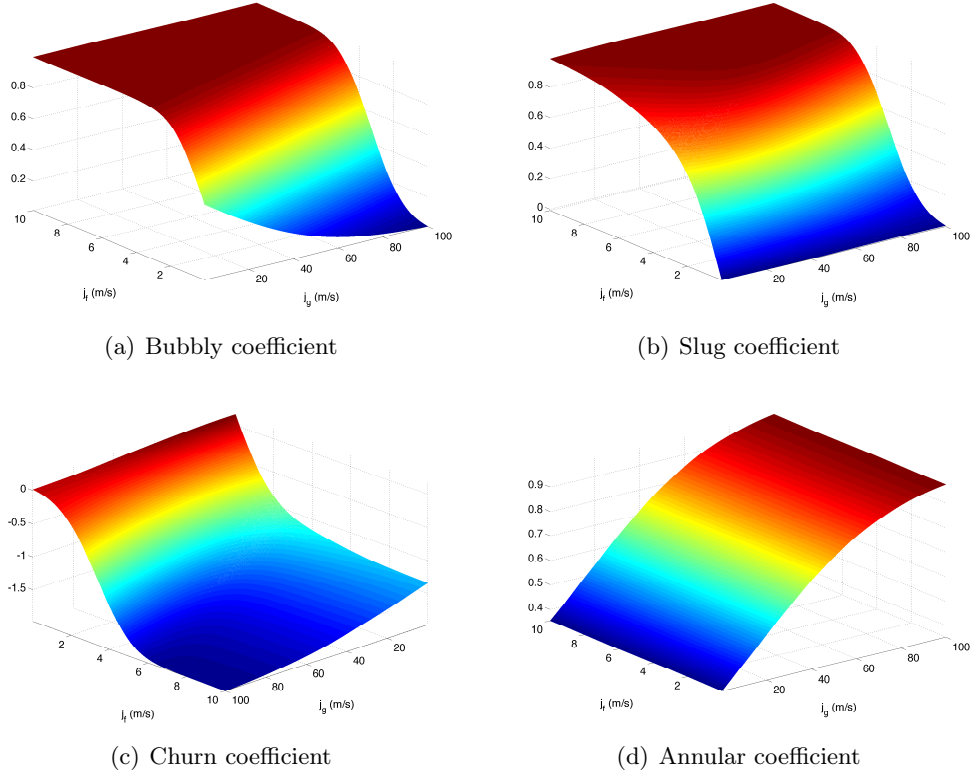
FIGURE 4.2: Void fraction's interpolation coefficients

$$f_{Annular} = \frac{1}{2} \left[1 + \mathrm{erf} \left(\frac{j_g - j_{f,CTA}}{\sigma \sqrt{2}} \right) \right] \tag{4.30}$$

$$f_{churn} = 1 - (f_{bubbly} + f_{slug} + f_{Annular}) \tag{4.31}$$

The subscript BTS refers to the transition bubbly $\rightarrow$ slug, CTS refers to the transition slug $\rightarrow$ churn and the subscript CTA refers to churn transition $\rightarrow$ annullar. The value of σ has been obtained by fitting the data from the database benchmark and is equal to $\sigma = 42.31$. Figure 4.2 shows the trends of the above functions for the values of j_g and j_f encountered in industrial applications.

To calculate the global void fraction coefficients were included in the global equations, here below. In Eq. (4.32) we calculate the void fraction derived from models for large

pipes, while Eq. (4.33) we calculate the void fraction derived from models for small pipes. The Eq. (4.34) combines the above equations.

$$\text{VF}_{large} = \frac{\sum_i \text{VF}_{i,large} f_{i,large}}{\sum_i f_{i,large}} \tag{4.32}$$

$$\text{VF}_{small} = \frac{\sum_i \text{VF}_{i,small} f_{i,small}}{\sum_i f_{i,small}} \tag{4.33}$$

Where $i = \{$bubbly, slug, churn e annular$\}$. And the global equation becomes:

$$\text{VF} = \frac{\text{VF}_{small} f_{small} + \text{VF}_{large} f_{large}}{f_{small} + f_{large}} \tag{4.34}$$

This type of approach (via the distribution functions) eliminates the problem of discontinuity in the transition zone given by a linear law [24] and is more suitable for 1D or 2D codes that exploit this model as a closure for the equations of motion, since the functions are $C^\infty(\mathbb{R})$.

4.3   Flow transition criteria

4.3.1   Churn to Annular transition

The transition from churn to annular is calculated obtaining a velocity value of the dispersed phase such that, overcoming it, we reach the annular regime. Ishii [4], postulated two different mechanisms that lead to the transition, both of which are derived from a balance of forces of the liquid, involving the surface tension and the drag force of the gas.

$$j_g|_{CTA} = \left(\frac{\Delta \rho g \sigma}{\rho_g^2} \right)^{1/4} N_{\mu_f}^{-0.2} \tag{4.35}$$

This criterion can also be used in large diameter pipes, according to Eqs. (4.36), because the diameter doesn't influence the transition boundary. At standard conditions the value of the minimum diameter is 5.91 cm.

$$D_h \geq \frac{\sqrt{\frac{\sigma}{\Delta \rho g}} N_{\mu_f}^{-0.4}}{\left(\frac{1-0.11C_0}{C_0}\right)^2}; \quad C_0 = 1.2 - 0.2\sqrt{\frac{\rho_g}{\rho_f}}; \quad N_{\mu_f} = \frac{\mu_f}{\sqrt{\rho_f \sigma \sqrt{\frac{\sigma}{g\Delta \rho}}}} \tag{4.36}$$

4.3.2 Slug to Churn transition

The transition between slug and churn is calculated using two models: one for small pipes and the other for intermediate and large pipes. For small pipes was proposed by Mishima and Ishii [10], in an implicit form.

$$\frac{jg}{C_0 j + 0.35\sqrt{\frac{gD_h\Delta \rho}{\rho_f}}} = 1 - 0.813 \left[\frac{(C_0 - 1)j + 0.35\sqrt{\frac{gD_h\Delta \rho}{\rho_f}}}{1 + 0.75\sqrt{\frac{gD_h\Delta \rho}{\rho_f}} \left(\frac{\Delta \rho g D_h^3}{\rho_f \nu_f^2}\right)^{1/18}} \right]^{3/4} \tag{4.37}$$

The transition was obtained by postulating that the void fraction in the region of interest exceed that in the section of the bubble to slug, using the Bernoulli equation integrated along the bubble slug. The length of the bubble has been converted from mechanical considerations regarding the behavior of the liquid film in the area of the tail of the bubble.

As the speed of a slug bubble was used the relationship derived from the work of Ishii [4].

$$v_{gs} = C_0 j + 0.35\sqrt{\frac{gD_h\Delta \rho}{\rho_f}} \tag{4.38}$$

According to Mishima and Ishii [10], the dimensionless group $\left(\Delta \rho g D_h^3 / \rho_f \nu_f^2\right)^{1/18}$ can be approximated at ≈ 3 for fluids with very low viscosity. In the following discussion we considered keep the size group to take into account also the effect of the diameter.
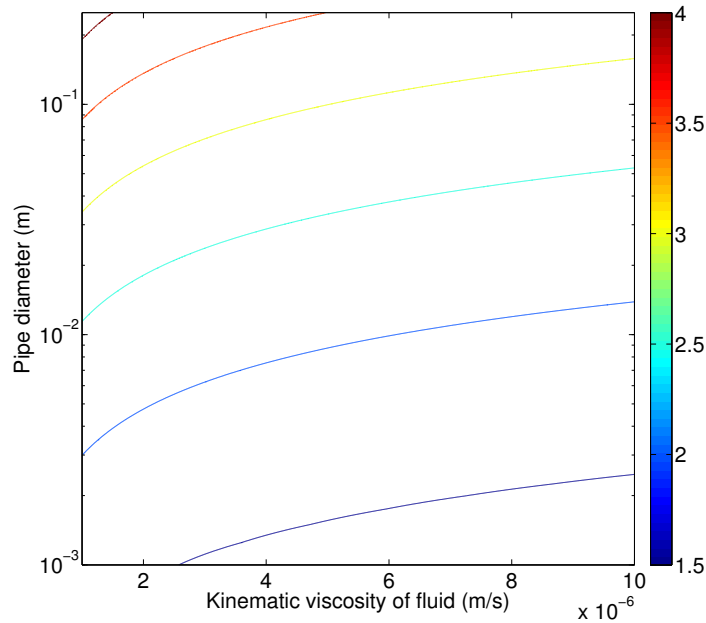
FIGURE 4.3: Dimensionless group

Figure 4.3 shows the dimensionless group in function of the diameter and the kinematic viscosity calculated at ambient conditions, for air-water. It can be noted how, in the case of pipes of small diameter, the value of the group approaches the unit value.

With regard to the transition to large pipes, the report given by Taitel et al. [17] in implicit form, is used in this model. It shows the fact that the term L/D_h refers to the dimensionless distance for which the profile has fluid totally developed and not the total length of the pipe. For large pipes the fully developed flow is obtained after five diameters.

$$\frac{L}{D_h} = 40.6 \left(\frac{j}{\sqrt{gD_h}} + 0.22 \right) \tag{4.39}$$

<center>TABLE 4.2: Employed models</center>

Pipe	Bubbly	Cap/Slug	Churn	Annular
Small	Hibiki and Ishii [5]	Ishii [4] Slug	Ishii [4] Churn	Kawanishi et al. [11]
Large	Shipley [7]	Mishima and Ishii [10] Slug	Clark and Flemmer [8] + Kawanishi et al. [11]	Hibiki and Ishii [12]

4.3.3 Bubbly to Slug transition

The transition from bubbly to slug is determined by statistical conditions, in which it is expected that the probability of coalescence between bubbles (assumed spherical) is very high. The threshold value is set at ≈ 0.3. This value can also be obtained from geometrical considerations, dictated by the maximum degree of packing of the bubbles (spheres) in a tetrahedral geometry [10]. Exploiting the model (4.50) theorized by Ishii [4] is obtained, by substitution, the relation between j_g e j_f for the transition bubbly to slug. The above equation is given, in the form common to all possible diameters, in explicit form.

$$j_f|_{bts} = 3j_g - 1.15 \left(\frac{\sigma g \Delta \rho}{\rho_f^2} \right)^{1/4} \tag{4.40}$$

4.4 Employed models

The models used were collected from the literature for both small pipes that for large pipes.

4.4.1 Large pipes

For the annular regime has been proposed the model of Hibiki and Ishii [12].

$$C_0 = 1.2 - 0.2 \left(\frac{\rho_g}{\rho_f} \right)^{1/2}; \quad v_{gj} = 3.0 \left(\frac{\sigma g \Delta \rho}{\rho_f^2} \right)^{1/4} \tag{4.41}$$

For the churn regime has been proposed a linear combination between the model of Clark-Flemmer (eq. 4.42) and the Hirao (eq. 4.47).

$$C_0 = 0.934(1 + 1.42 \langle \alpha \rangle); \quad v_{gj} = 1.53 \left(\frac{\sigma g}{\rho_f} \right)^{1/4} \tag{4.42}$$

For the slug regime was used to model the Mishima and Ishii [10].

$$C_0 = 1.2 - 0.2 \left(\frac{\rho_g}{\rho_f} \right)^{1/2} \tag{4.43}$$

$$\begin{cases} v_{gj} = 0.03 \left(\dfrac{\rho_g}{\rho_f} \right)^{-0.157} N_{\mu_f}^{-0.562} \left(\dfrac{\sigma g \Delta \rho}{\rho_f^2} \right)^{1/4} & \text{se } N_{\mu_f} \leq 2.25 \times 10^{-3} \\[3mm] v_{gj} = 0.92 \left(\dfrac{\rho_g}{\rho_f} \right)^{-0.157} \left(\dfrac{\sigma g \Delta \rho}{\rho_f^2} \right)^{1/4} & \text{se } N_{\mu_f} > 2.25 \times 10^{-3} \end{cases} \tag{4.44}$$

For the bubbly regime was used to model the Shipley [7].

$$C_0 = 1.2; \quad v_{gj} = 0.24 + 0.35 \left(\frac{j_g}{j} \right)^2 \sqrt{g D_h \langle \alpha \rangle} \tag{4.45}$$

4.4.2 Small pipes

For the annular regime has been proposed the model developed by Kawanishi et al. [11].

$$C_0 = 1.2 - 0.2 \sqrt{\frac{\rho_g}{\rho_f}} \tag{4.46}$$

$$\begin{cases} v_{gj} = 0.52 \left(\sqrt{\dfrac{D_h g \Delta \rho}{\rho_f}} \right)^{1/2} & \text{se } j > 0.24 \text{ m/s} \\[4mm] v_{gj} = \dfrac{1}{2} \left[0.52 \left(\sqrt{\dfrac{D_h g \Delta \rho}{\rho_f}} \right)^{1/2} + \sqrt{2} \left(\dfrac{\sigma g \Delta \rho}{\rho_f^2} \right)^{1/4} \right] & \text{se } j \leq 0.24 \text{ m/s} \end{cases} \tag{4.47}$$

For the churn regime has been proposed the model developed by Ishii [4], part of the same work for its models above.

$$C_0 = 1.2 - 0.2 \sqrt{\frac{\rho_g}{\rho_f}}; \qquad v_{gj} = \sqrt{2} \left(\frac{\sigma g \Delta \rho}{\rho_f^2} \right)^{1/4} (1 - \langle \alpha \rangle)^{1/4} \tag{4.48}$$

For the slug regime was proposed the model developed by Ishii [4].

$$C_0 = 1.2 - 0.2 \sqrt{\frac{\rho_g}{\rho_f}}; \qquad v_{gj} = 0.35 \sqrt{\frac{D_h g \Delta \rho}{\rho_f}} \tag{4.49}$$

For the bubbly regime has been proposed the model developed by Hibiki and Ishii [5].

$$C_0 = 1.2 - 0.2 \sqrt{\frac{\rho_g}{\rho_f}}; \qquad v_{gj} = \sqrt{2} \left(\frac{\sigma g \Delta \rho}{\rho_f^2} \right)^{1/4} (1 - \langle \alpha \rangle)^{7/4} \tag{4.50}$$

4.5 Model validation

A number of databases have been used to validate and correct the model, a part of them are relative to large pipes, another part for the small pipes. The parameters used for the estimate of the error between the model results and the benchmark database are: the mean, standard deviation, and the mode of the relative error, calculated as the absolute value of the difference between the calculated void fraction in relation to void fraction obtained experimentally, an ultimate parameter of goodness is the mean square error (RMSE).

TABLE 4.3: RMSE of literature models with database large pipes

Benchmark	Models			
database	Clark/Flemmer [8]	Hills [6]	Kawanishi et al. [11]	Hibiki and Ishii [12]
Hill	0.0907	0.0272	0.0437	0.0726
Hashemi	0.1047	0.0631	0.0756	0.0645
Hall	0.1608	0.1992	0.1811	0.1735
Smith 4"	0.1160	0.1753	0.1498	0.1555
Smith 6"	0.0863	0.0971	0.1154	0.1215
Hsu	0.2269	0.3356	0.2978	0.3035
Inoue	0.0783	0.1715	0.1092	0.0921
Yoneda	0.0783	0.1091	0.1016	0.1037
Stankovic	0.0771	0.0279	0.0395	0.0670
Schlegel	0.1215	0.0807	0.0794	0.0870

Benchmark	Models		
database	Mishima and Ishii [10]	Shipley [7]	Overall
Hill	0.0856	0.0292	0.0582
Hashemi	0.0726	0.0862	0.0778
Hall	0.1922	0.1891	0.1827
Smith 4"	0.1615	0.1351	0.1489
Smith 6"	0.1256	0.0989	0.1075
Hsu	0.3046	0.2990	0.2946
Inoue	0.0886	0.0964	0.1060
Yoneda	0.0936	0.0840	0.0951
Stankovic	0.0765	0.0323	0.0534
Schlegel	0.0798	0.0755	0.0873

The first step to assess the goodness of the model was to evaluate the performance of the individual models in the literature to calculate the void fraction for all benchmark database and the results are shown in Table 4.3. Then we calculated the void fraction through the proposed model.

In general, the drift-flux models takes from literature have a quite satisfactory performances, because some of these are derived from mechanistic consideration. The main problem is the applicability outside their effective range. The aim of the proposed model is to merge the drift-flux model especially designed for a particular flow regime, to extend the applicability.

TABLE 4.4: Database large pipes

| Author	Fluids	D_h (cm)	j_g (m/s)	j_f (m/s)	$\langle \alpha \rangle$ (%)
Hills [6]	A/W	15.0	$0.030 - 3.500$	$0.000 - 2.600$	$5.43 - 53.85$
Hashemi et al. [26]	A/W	30.5	$0.010 - 1.160$	$0.000 - 0.600$	$0.90 - 93.40$
Hall et al. [27]	steam/W	17.1	$0.117 - 0.740$	$0.021 - 0.208$	$11.40 - 91.10$
Smith et al. [28]	A/W	10.6	$0.048 - 8.790$	$0.050 - 2.000$	$1.84 - 71.44$
Smith et al. [28]	A/W	15.2	$0.040 - 1.140$	$0.050 - 1.000$	$1.00 - 39.32$
Hsu et al. [29]	N_2/W	10.2	$3.171 - 15.832$	$3.890 - 19.839$	$3.60 - 22.00$
Inoue [30]	A/W	20.0	$0.003 - 4.066$	$0.035 - 0.274$	$3.00 - 46.50$
Yoneda et al. [31]	steam/W	15.5	$0.010 - 0.250$	$0.210 - 0.590$	$3.78 - 34.62$
Stankovic [32]	A/W	15.2	$0.021 - 0.674$	$0.000 - 0.755$	$2.71 - 40.59$
Schlegel [14]	A/W	15.0	$0.100 - 5.100$	$0.050 - 1.000$	$9.11 - 82.89$

4.5.1 Large pipes

The databases used for validation of the "large pipes" part of the algorithm is reported in Table 4.4. The employed fluids are, mainly, air and water at standard condition of pressure and temperature. For Hill and Hashemi, inlet and outlet sections are horizontal and the test section is vertical. For Hall, the facility is vertical and the steam is injected at the pressure condition of 4.4 MPa. Smith have a bubble generator with porous sparger. Hsu have a facility with a hook shape. Yoneda generates the steam with a bundle of heated rods at an unknown conditions. In Table 4.5 is reported the goodness of the proposed model, while in figure 4.4 show the comparison between experimental void fraction and the computed one.

It was observed that the overall RMSE is slightly lower than the lowest RMSE obtained with the original model. The lowest RMSE within the databases are obtained for Hill, Stankovich and Hashemi. In fact, they have the smallest error average. The smallest dispersion of point (measured by the standard deviation) are for Hill, Stankovich and Yoneda. Sometimes the model does not respond very well with fluids other than the air and water, in fact, for the cases of Hall, the model underestimates the void fraction; vice versa for the case with nitrogen instead of air, this because all of the employed models are designed for air-water mixture. The slight deviation from the center line of the rest of the Smith, Yoneda and Inoue databases is due to disturbed experimental

TABLE 4.5: Relative error of the proposed model for large pipes

Database	Mean	Std. Dev.	Mode	RMSE
Hall	26.8	18.1	1.1	0.1841
Hashemi	16.1	36.2	1.6	0.0615
Hill	11.0	9.2	0.4	0.0446
Hsu	248.1	79.7	143.4	0.3261
Inoue	56.5	44.9	0.5	0.0931
Schlegel	18.9	14.3	0.0	0.0793
Smith 6"	76.8	262.3	0.6	0.1090
Stankovich	14.0	11.7	0.2	0.0471
Yoneda	44.2	6.2	37.7	0.0935
Smith 4"	65.5	245.8	0.3	0.1532
Overall	57.8	72.8	18.6	0.1192

measurements, because their are taken with the optical probe (very delicate instrumentation and less accurate if the calibration is not employed correctly). May be interesting to observe that, for a given database (thus taking into account the properties and operating conditions rather than the nature of the model), the performance of different models can change. In particular, the proposed model responds better than the average of the models in the literature, for the 60% of cases.

The main failure of this model is that it uses models that do not work well with fluids other than air and water. For example, if you are using steam, the model underestimates the actual void fraction. In particular, you may have problems in case of high operating pressure. Working fluids such as nitrogen and oxygen lead to an overestimation of the void fraction.

4.5.2 Small pipes

The databases used for validation of the "small pipes" part of the algorithm is reported in Table 4.6. The employed fluids are, mainly, air and water at standard condition of pressure and temperature with an addiction of alcohol and glycerine. Bhagwat and Ghajar [18] collected a database for vertical upward and downward configurations and, also, for horizontal arrangement at 2 bar. Griffith and Snyder [23] have conduced
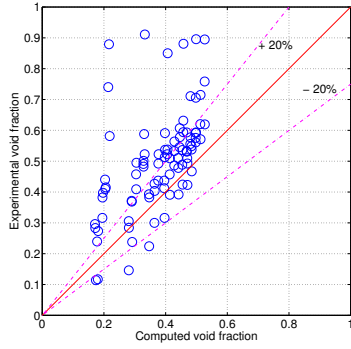
(a) Hall data
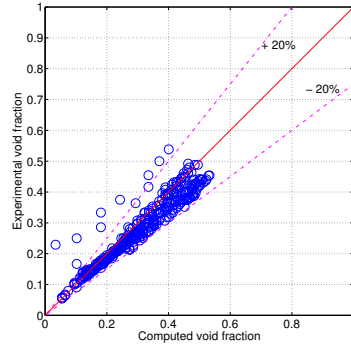
(b) Hill data
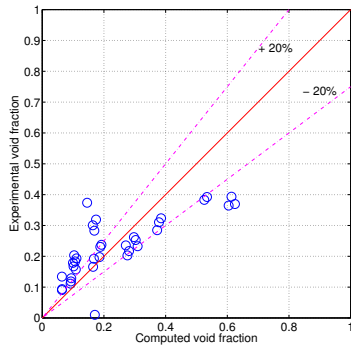
(c) Smith 6" data
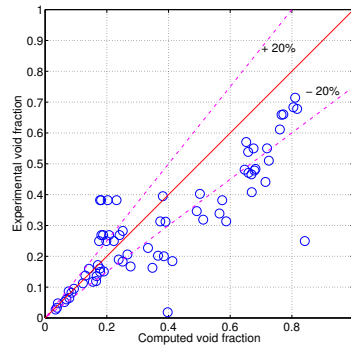
(d) Smith 4" data
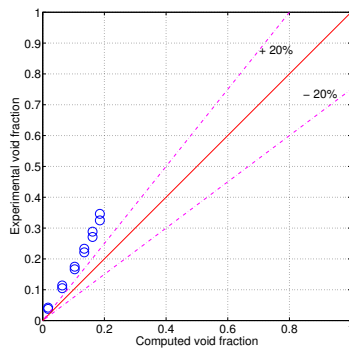
(e) Yoneda data

FIGURE 4.4: Graphs of model goodness for large pipes
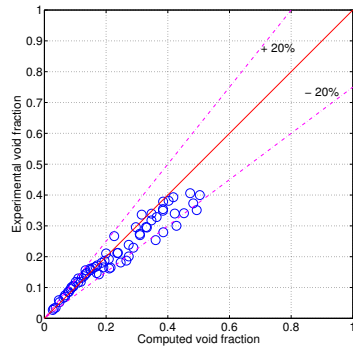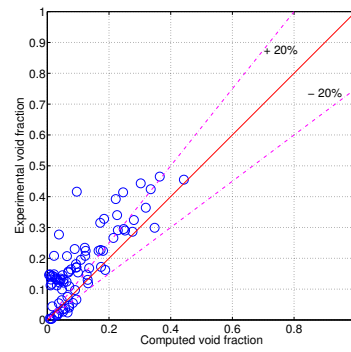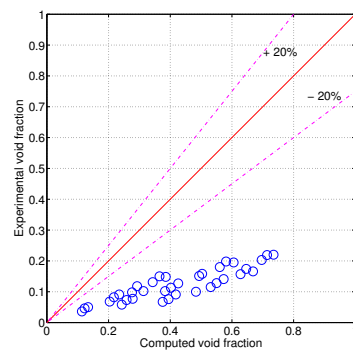
(a) Stankovich data
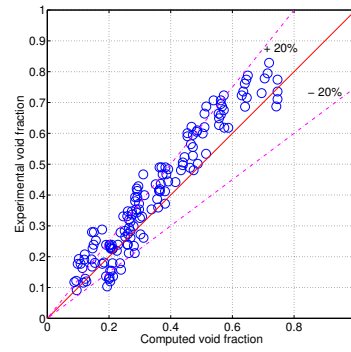
(b) Schlegel data
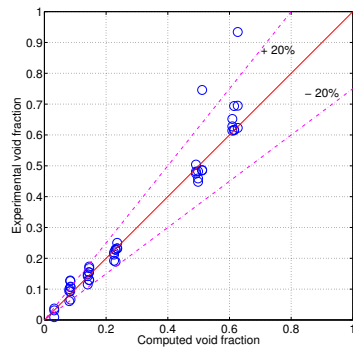
(c) Hashemi data

(d) Inoue data

(e) Hsu data

FIGURE 4.5: Graphs of model goodness for large pipes (continue)

TABLE 4.6: Database small pipes

Author	Fluids	D_h (cm)	j_g (m/s)	j_f (m/s)	$\langle\alpha\rangle$ (%)
Griffith [23]	A/W	1.27	2.893 − 61.57	0.001 − 1.670	65.80 − 98.20
	A/W/alcohol	1.27	7.803 − 40.69	0.198 − 0.655	79.00 − 90.30
	A/W/glycerine	1.27	5.578 − 38.74	0.000 − 0.765	81.20 − 90.00
	CO_2/W	1.27	5.197 − 28.01	0.118 − 0.988	75.90 − 92.30
	A/W	2.54	7.254 − 26.52	0.000 − 0.448	81.30 - 96.20
	A/W/alcohol	2.54	13.93 − 15.48	0.240 − 0.249	85.70 − 86.40
	A/W/glycerine	2.54	9.266 − 16.76	0.150 − 0.320	82.50 − 87.00
	A/W	3.81	0.506 − 18.23	0.007 − 0.375	50.00 − 94.70
Ghajar [18]	A/W	1.27	0.431 − 20.03	0.080 − 1.170	15.50 − 89.83

an extensive experimental campaign with multi-fluids vertical upward arrangement, in small pipes.

In Table 4.7 is reported the goodness of the proposed model with the small pipe, while in figure 4.6 the comparison between experimental void fraction and the computed one for the main fluids database.

The database analyzed refer to portions of the flow field at high void fraction this allows to reduce calculation errors (since they are calculated as the ratio between the difference of the database and the original database). All cases get good performance, also employing fluids other than air and water. It should be noted a certain underestimation of the value of the void fraction at very high air flow rates. Ghajar data is the most wide of the entire databases and it's range from 0.2 to 0.9 void fraction. The model respond very well even in the region below the annular pattern (only recognized by Griffith's database), then the model chosen for small pipe regime is good. The overall RMSE is low and the RMSE for the Ghajar's database is lower that the lowest RMSE for entire large pipe's databases. Even in this case, the model appears to work very well.
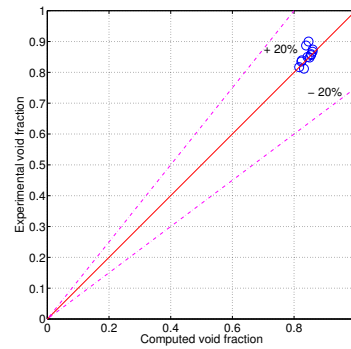
4.5.3 Other configurations

There are a some databases, which have a different flow configuration, that have been tested with the proposed model. Both of them are from Bhagwat and Ghajar [18]: one

TABLE 4.7: Relative error of the proposed model for small pipes

Database	Fluids	D_h (cm)	Mean	Std. Dev.	Mode	RMSE
Griffith [23]	A/W	1.27	3.6	2.9	0.1	0.0419
	A/W/alcohol	1.27	2.6	1.3	0.3	0.0253
	A/W/glycerine	1.27	1.7	2.0	0.0	0.0225
	CO_2/water	1.27	3.7	1.4	0.9	0.0329
	A/W	2.54	5.1	3.3	0.2	0.0558
	A/W/alcohol	2.54	2.8	0.2	2.7	0.0241
	A/W/glycerine	2.54	1.6	1.3	0.2	0.0174
	A/W	3.81	3.2	2.8	0.1	0.0370
Ghajar [18]	A/W	1.27	11.2	10.0	0.2	0.0622
Overall	-	-	3.9	2.8	0.5	0.0355
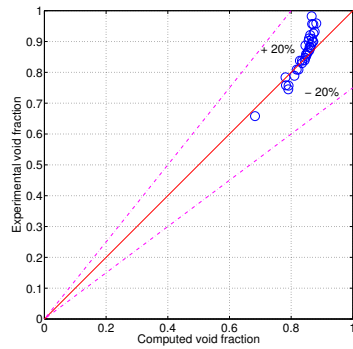
(a) Griffith data

(b) Griffith (glycerine) data
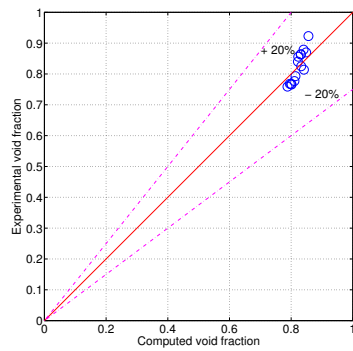
(c) Griffith (CO_2) data
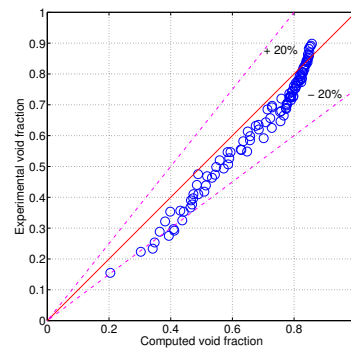
(d) Ghajar data

FIGURE 4.6: Graphs of model goodness for small pipes

TABLE 4.8: Other configuration database

Author	Configuration	j_g (m/s)	j_f (m/s)	$\langle\alpha\rangle$ (%)
Ghajar [18]	Horizontal	$0.170 - 12.96$	$0.140 - 0.960$	$17.50 - 84.33$
Ghajar [18]	Downward	$0.101 - 15.23$	$0.120 - 2.180$	$4.800 - 90.00$

TABLE 4.9: Relative error of the proposed model for other configurations

Author	Configuration	Mean	Std. Dev.	Mode	RMSE
Ghajar [18]	Horizontal	9.2602	9.113	0.0837	0.0564
Ghajar [18]	Downward	6.3934	6.6012	0.181	0.0414
Polimi	Countercurrent	46.4703	7.7391	32.1176	0.0668

is for downward configuration and the other is for horizontal arrangement at 2 bar and $D_h = 1.27$ cm (Tab. 4.8).

Even in this case, the proposed model, give a good results (Tab. 4.9 and Fig. 4.7). The mean of relative error is lower than 10%. The agreement with the experimental data is excellent because the computed points are inside the 20% error lines (magenta lines).

Even the database from our laboratory was used to test the proposed model. The calculated void fraction slightly underestimate the real one because the test configuration is countercurrent and the drift velocity between the two fluids is greater than for the upward configuration. The model used here are designed for upward and downward configuration. However, the standard deviation is low and RMSE is similar to the horizontal solution. In this last case, the flow structures are very different from the case of vertical pipes.

In Fig. 4.8 is reported the flow chart of this model. First, the data must be loaded. The final result is the computed void fraction (α_{com}). *CTA, STC and BTS* are the acronyms for the transitions from Churn to Annular, from Slug to Churn and from Bubbly to Slug, respectively. D_{SI} and D_{IL} stay for transitional diameter from small to intermediate and for intermediate to large, respectively. σ_r and σ_d are the setting parameters of transitional model of flow regime and diameter, respectively.
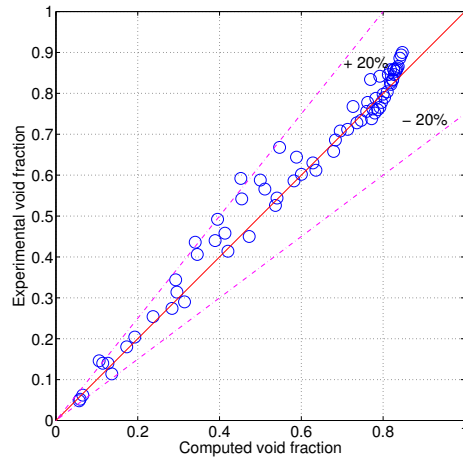
(a) Downward data
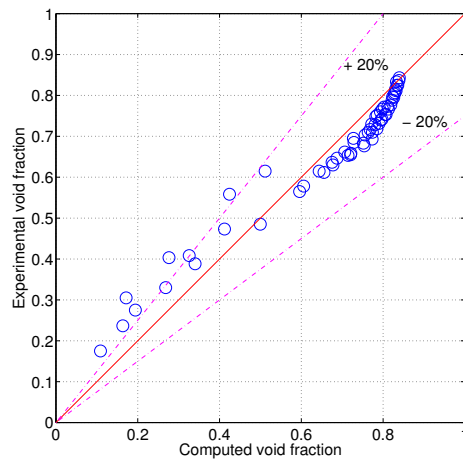
(b) Horizontal data
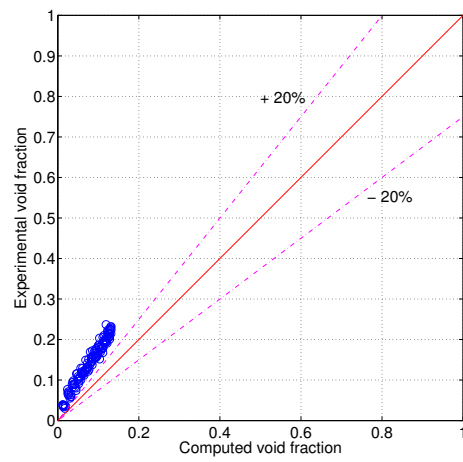
(c) Polimi data

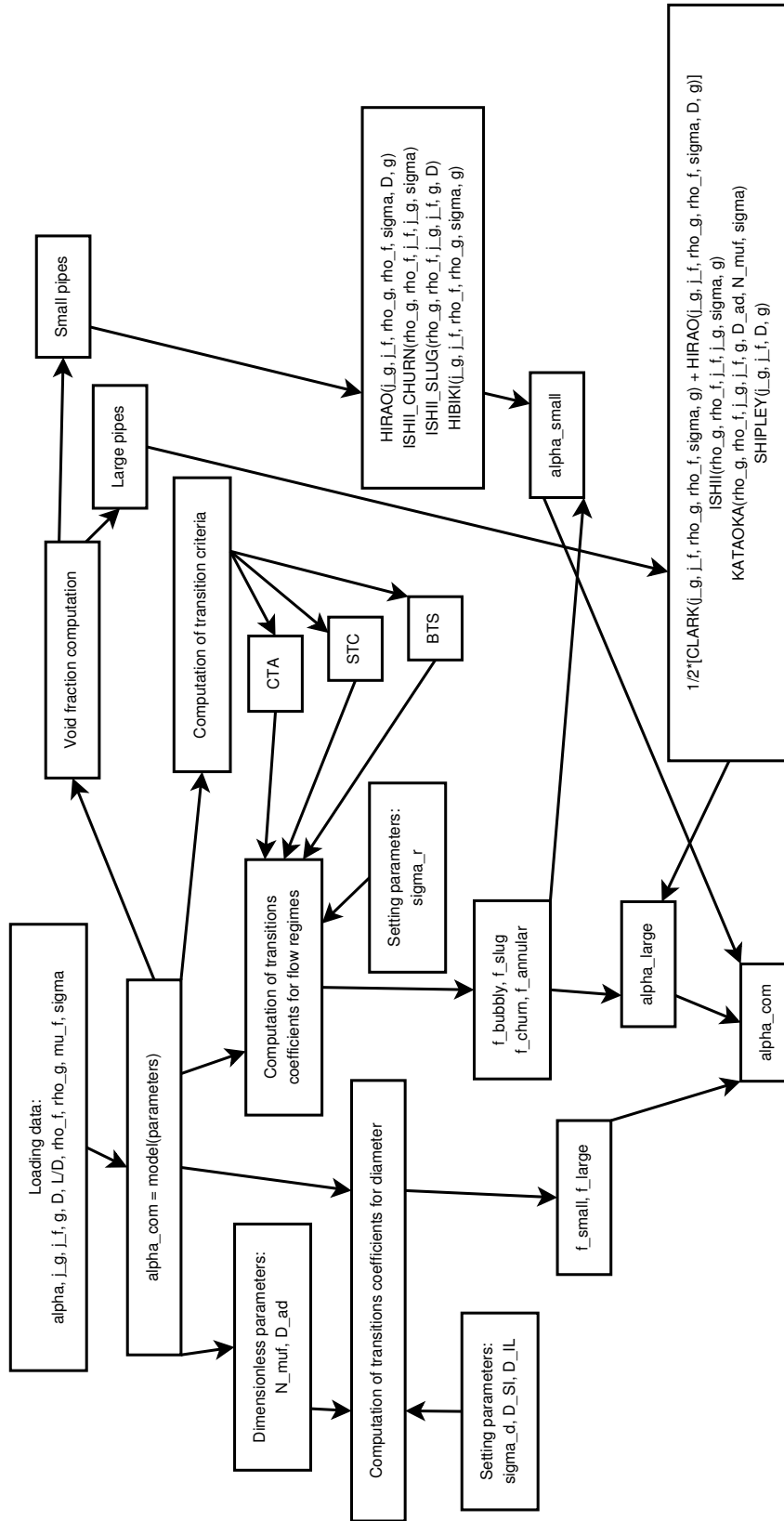FIGURE 4.7: Graphs of model goodness for other configuration

FIGURE 4.8: Flow chart of comprehensive model

Chapter 5

NOVEL DRIFT FLUX MODEL FOR COUNTER-CURRENT FLOWS IN LARGE DIAMETER PIPES

The aim of the proposed model is to correlate the data collected in the laboratory by a drift-flux modeling and develop a new model for very large pipes ($D_h^* > 80$). The semi-empirical coefficients are developed in polynomial form and properly fitted with the experimental data. The model was tested with data from several studies, all inherent in bubble columns, because to the difficulty of finding the countercurrent experimental data in literature.

5.1 Model conceptual idea

Starting from the definition of drift-flux model, proposed by Zuber and Findlay [13] – shown in Eq. (5.1) – it's possible to recognize that the actual speed of the gas (v_g) depends linearly on the total volumetric flux (j) through the distribution parameter (C_0) and the drift velocity (v_{gj}).

$$v_g = \frac{j_g}{\alpha} = C_0 j + v_{gj} \tag{5.1}$$

The method proposed by several authors in the world, in order to obtain the value of the two parameters of the model, is to plot the ratio j_g^+/α as a function of dimensionless total flow rate, j^+. The data will assume a roughly linear trend and provide, for $j^+ = 0$ the value of v_{gj}^+, and C_0 the resulting value j_g^+/α. The dimensionless approach is very useful because it allows you to manipulate pure numerical values. The dimensionless group adopted in this model is due to the Kutateladze and it use the formulation of the Taylor wavelength, Eq. (5.2). A different approach is to employ the Wallis dimensionless group, which depends on a characteristic length of the system which is not always uniquely definable and therefore was discarded.

$$K_{kutateladze} = \left(\frac{g\sigma\Delta\rho}{\rho_g^2}\right)^{-\frac{1}{4}}; \qquad K_{wallis} = \left(\frac{gL_c\Delta\rho}{\rho}\right)^{-\frac{1}{2}} \tag{5.2}$$

Through this process, the two parameters of the model are derived for each condition of superficial velocity of the liquid. Subsequently, the data obtained are interpolated to connect model parameters with the surperficial velocity of the liquid. Finally, to include the variability in density with respect to environmental conditions, a formulation has been adopted for the distribution parameter that takes into account the relationship between the densities of the two fluids used in the system.

5.2 Numerical model

The database used for setting the model has been obtained experimentally in the laboratories of the Polytechnic of Milan. Were collected the data of void fraction for a total of 130 operating points at different flow rates of liquid and gas. The techniques used for data acquisition are: global measurement of the volumes of air and water that circulates in the system and local measurement by optical probes. The database chosen for model setting is determined by measuring the global void fraction (since these values are averaged over the whole system and then the main uncertainty can be limited to the measuring system and not caused by local fluctuations at turbulence scale). The value of v_g^+ was derived from the ratio of the dimensionless volumetric gas flux using Eq. (5.2), and the values of void fraction in the database. The total flow

(a) Regime: *bubbly*
$Q_g = 20\ N\mathrm{dm}^3\,\mathrm{min}^{-1}$
$Q_f = 26.7\ \mathrm{dm}^3\,\mathrm{min}^{-1}$

(b) Regime: *churn bubbly*
$Q_g = 200\ N\mathrm{dm}^3\,\mathrm{min}^{-1}$
$Q_f = 200\ \mathrm{dm}^3\,\mathrm{min}^{-1}$

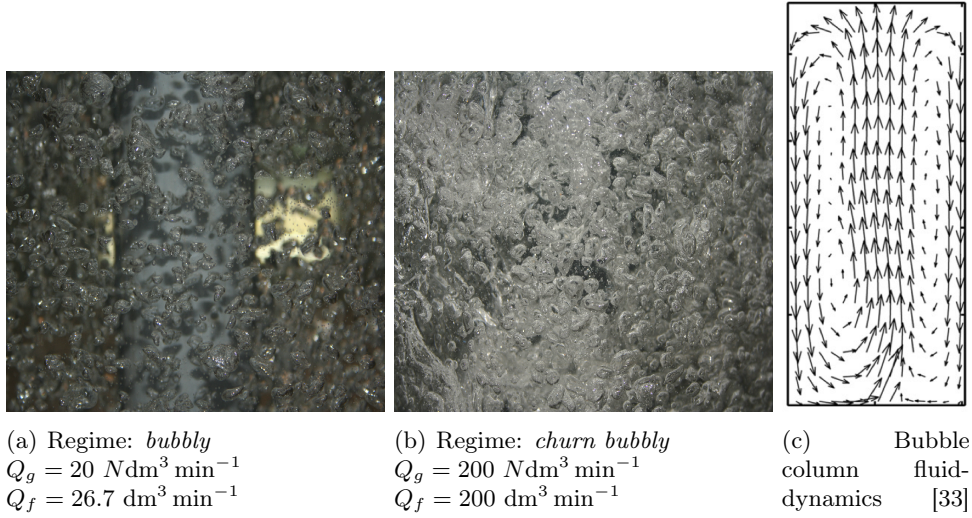(c)　　　　Bubble column　　fluid-dynamics　　[33]

FIGURE 5.1: Pictures of the flow regime, from our experimental facility

was taken as the difference of the dimensionless volumetric flow of the two fluids, only to accounting for the countercurrent direction of the fluids.

The data fitting to the linear model was run for ten liquid flow and has produced two vectors: one containing the values of C_0 and the other containing the values of v_{gj}. The sub-model used to link the drift velocity to the volumetric flow of liquid is linear. The model that binds the distribution parameter to j_f^+ is also linear and includes the effect of pressure by the ratio between the densities of the two fluids. In this regard, the work of Hibiki and Ishii [12] has inspired me in the formulation of C_0, which resembles at one of their large diameter's regimes: *bubbly or cap bubbly*, In our facility, we had observed precisely these flow regimes (Fig. 5.1).

$$\begin{cases} C_0 = \left(a_1 j_f^+ + a_2\right)\left(1 - \sqrt{\dfrac{\rho_g}{\rho_f}}\right) + \sqrt{\dfrac{\rho_g}{\rho_f}} \\ v_{gj}^+ = b_1 j_f^+ + b_2 \end{cases} \tag{5.3}$$

After the data fitting, the numerical values of the model coefficients are (with 95% confidence bound):

- $a_1 = 20.2784\,(13.73, 25.42)$

- $a_2 = 2.4936\,(2.377, 2.507)$

- $b_1 = 2.1701\,(2.01, 2.331)$

- $b_2 = 0.0274\,(0.02564, 0.02919)$

5.3   Model validation

For the model validation are employed database of bubble columns (that employ working fluids such as air and water) taken from literature (Table 5.1). The main limitation of these data is that only cover the velocity fields in which the velocity of the fluid is equal to zero, while this model would need a flow field even richer than that obtained in our laboratories.

The advantage of employing database benchmark derived from the bubble columns is in the fact that their fluid dynamics is qualitatively similar to that present in the countercurrent configurations. The motion of the air that rises vertically, generates recirculation of liquid downward, to the sides of the column, the velocity profile performs well this phenomenon as shown in Fig 5.1(c).

TABLE 5.1: Bubble column database

Author	Year	Pipe type	D_h (cm)	j_g (m/s)	$\langle\alpha\rangle$ (%)
Studley [34]	2010	Circular	10.2	$0.005 - 0.200$	$0.300 - 26.84$
Simonnet et al. [35]	2008	Rectangular	6.67	$0.005 - 0.082$	$2.160 - 19.05$

The model does not work not very well for very low values of void fraction (i.e. low values of gas velocity), probably because the model setting is derived from a flow map with a small set of measurement at liquid velocity equal to zero. There is a systematic deviation to high experimental void fraction not to "at favor to safety", probably due to the error on the calculation of real gas volumetric flux.

TABLE 5.2: Relative error of the proposed C-C model for bubble column's database

| Author	Mean	Std. Dev.	Mode	RMSE
Studley [34]	30.65	19.73	16.42	0.0757
Simonnet et al. [35]	26.14	7.53	16.03	0.0167
Overall	28.40	13.63	16.22	0.0462
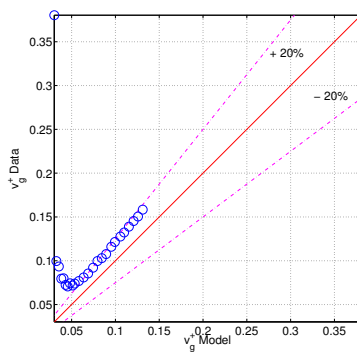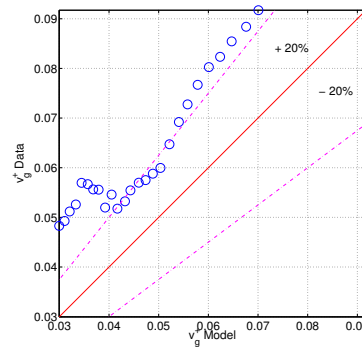
(a) Studley [34] (b) Simonnet et al. [35]

FIGURE 5.2: Graphs of model goodness for bubble columns

5.4   Conclusions

The linear fit of the two parameters (see Fig 5.3(a)) has been chosen based on considerations of robustness of the model, computational speed and to minimize the mean square error. Indeed, the fact that it is used a linear model for the distribution parameter affects very little on the calculation of the model (less than 5 %), even if the profile of this parameter is generally not linear (sum of exponentials). This stems from the fact that the fashion of the maximum values of the dimensionless liquid volumetric flow rates in the various experimental plants collected from the literature (see previous sections) was approximately the value of 0.0227, which is very close to the maximum value found in our plant (0.0189). In the case that the mode value is exceeded, it is necessary to modify the formulation of the C_0, by introducing a nonlinear model as the sum of exponential polynomials or fractional, not without the introduction of errors especially when the database is not able to cover the whole range of operation required for a proper fit.

Overall, the model reflects well the Polimi database, with a relative error average of 4.33%, a standard deviation of 3.18 and a RMSE of 0.0021 (see Figure 5.3). All the values are within the error band $\pm 20\%$, in particular the maximum error does not exceed 14%. As for the databases used for validation of the model, we can not firmly say that the results are quite satisfactory. The main reason lies in the fact that the geometry of the validation databases is not the same of our facility, in fact, in the literature, there is often a configuration with a rectangular section (instead of circular).
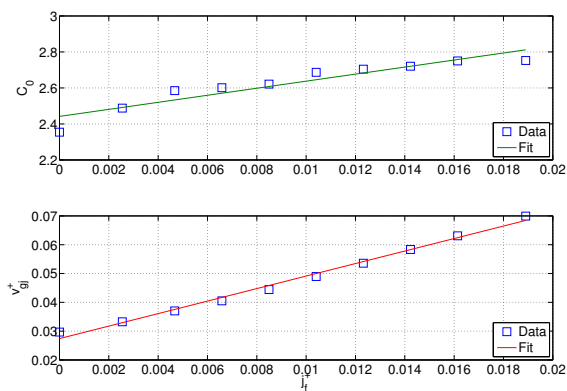
(a) Parameters fitting (C_0 e v_{gj})
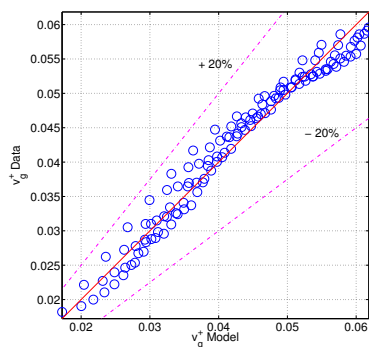
(b) Experimental data vs. calcolate void fraction (dimensionless)
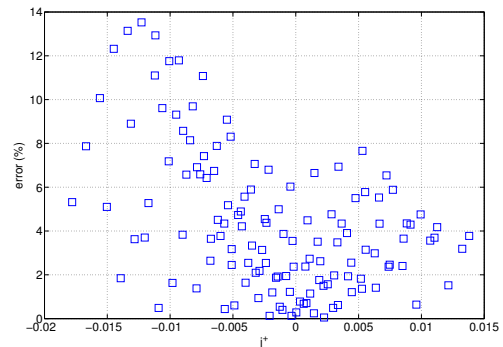
(c) Relative error

FIGURE 5.3: Model performance with Polimi database

Chapter 6

CONCLUSIONS AND FUTURE DEVELOPMENTS

In general, the research for correlations for the calculation of the void fraction find the utility in the calculation of the head losses in the piping, in fact the term of the gravitational acceleration is a function of void fraction. Knowing the flow regime on the basis of operating conditions is important (especially in the transport of crude oil) because, the regime that is established in the pipeline, may arise various problems: unwanted vibrations, malfunction of the air/water separator and fall down of the efficiency of the pumps. Other effects influenced by the void fraction are corrosion and erosion, arise mainly from the condition of turbulent slug regime. So it is important to have a model that can calculate the void fraction quickly and in a compact way, as a function of the properties of fluids and operating conditions.

Much more work can be conducted in the field of two-phase fluid dynamics of large pipes and, in particular, for this configuration in the laboratories of the Politecnico di Milano. The basis for a future development in the facility are the evaluation of mass exchange and heat exchange between phases in order to found the better configuration of sparger's holes in number and size (for the minimum bubbles diameter), and expand the physical conditions inside the test section: employ different gases and liquid (i.e. CO_2 and oil) in order to evaluate the erosion and corrosion mechanism; change the pressure and temperature to get closer to the downwell conditions. Any other efforts can be made about: high flow conditions in order to found the flooding conditions; change

the facility configuration to test the horizontal one and verify the model proposed in this thesis.

List of Figures

List of Tables

Symbols

f	Subscript. Indicate the liquid phase	
m	Subscript. Indicate the whole mixture	
$*, +$	Superscript. Indicate the dimensionless propriety	

D_h	Hydraulic diameter	m
g	Acceleration due to gravity	$\mathrm{m\,s^{-2}}$
d_s	Sauter mean diameter	m
$\langle F \rangle$	Area-averaging of propriety F	–
$\langle\langle F \rangle\rangle$	Void fraction weighted averaging of propriety F	–
A	Generical area	$\mathrm{m^2}$
v	Phase velocity	$\mathrm{m\,s^{-1}}$
j	Volumetric flux or superficial velocity	$\mathrm{m\,s^{-1}}$
v_{gj}	Drift velocity	$\mathrm{m\,s^{-1}}$

σ	Surface tension	$\mathrm{N\,m^{-1}}$
$\Delta\rho$	Difference between liquid and gas densities	$\mathrm{kg\,m^{-3}}$
μ	Dynamic viscosity	$\mathrm{Pa\,s}$
α	Void fraction	–
ρ	Fluid density	$\mathrm{kg\,m^{-3}}$
Γ_g	Mass transfer coefficient	$\mathrm{kg\,m^{-3}\,s^{-1}}$

Bibliography

[1] N. K. Omebere-Iyari, B. J. Azzopardi, and Y. Ladam. The identification of two-phase flow patterns and their transitions in large diameter vertical pipes at elevated pressures. *Am. Inst. Chem. Eng. J.*, 53:2493–2504, 2007.

[2] S. Benattalah, F. Aloui, and M. Souhar. Experimental analysis on the counter-current dumitrescu-taylor bubble flow in a smooth vertical conduct of small diameter. *Journal of Applied Fluid Mechanics*, 4(ISSN 1735-3572, EISSN 1735-3645): 1–14, 2011.

[3] Niels Deen, Bjørn Hjertager, and Solberg Tron. Comparison of piv and lda measurement methods applied to the gas-liquid flow in a bubble column. 2000.

[4] Mamoru Ishii. One-dimensional drift–flux model and constitutive equations for relative motion between phases in various two-phase flow regimes. 1977.

[5] T. Hibiki and M. Ishii. Distribution parameter and drift velocity of drift-flux model in bubbly flow. *International Journal of Heat and Mass Transfer*, 45(4):707 – 721, 2002. ISSN 0017-9310. doi: http://dx.doi.org/10.1016/S0017-9310(01)00195-8. URL `http://www.sciencedirect.com/science/article/pii/S0017931001001958`.

[6] J.H. Hills. The operation of a bubble column at high throughputs: I. gas holdup measurements. *The Chemical Engineering Journal*, 12(2):89 – 99, 1976. ISSN 0300-9467. doi: http://dx.doi.org/10.1016/0300-9467(76)87002-5. URL `http://www.sciencedirect.com/science/article/pii/0300946776870025`.

[7] DG Shipley. Two phase flow in large diameter pipes. *Chemical Engineering Science*, 39(1):163–165, 1984.

[8] NN Clark and RL Flemmer. Predicting the holdup in two-phase bubble upflow and downflow using the zuber and findlay drift-flux model. *AIChE journal*, 31(3): 500–503, 1985.

[9] G Kocamustafaogullari and M Ishii. Maximum fluid particle size for bubbles and drops. In *ASME Winter Annual Meeting, Miami Beach, Nov*, pages 17–22, 1985.

[10] Kaichiro Mishima and Mamoru Ishii. Flow regime transition criteria for upward two-phase flow in vertical tubes. *International Journal of Heat and Mass Transfer*, 27(5):723 – 737, 1984. ISSN 0017-9310. doi: http://dx.doi.org/10.1016/0017-9310(84)90142-X. URL `http://www.sciencedirect.com/science/article/pii/001793108490142X`.

[11] Kouhei Kawanishi, Yasuhiko Hirao, and Ayao Tsuge. An experimental study on drift flux parameters for two-phase flow in vertical round tubes. *Nuclear Engineering and Design*, 120(2–3):447 – 458, 1990. ISSN 0029-5493. doi: http://dx.doi.org/10.1016/0029-5493(90)90394-D. URL `http://www.sciencedirect.com/science/article/pii/002954939090394D`.

[12] Takashi Hibiki and Mamoru Ishii. One-dimensional drift–flux model for two-phase flow in a large diameter pipe. *International Journal of Heat and Mass Transfer*, 46(10):1773 – 1790, 2003. ISSN 0017-9310. doi: http://dx.doi.org/10.1016/S0017-9310(02)00473-8. URL `http://www.sciencedirect.com/science/article/pii/S0017931002004738`.

[13] N. Zuber and J. A. Findlay. Average volumetric concentration in two-phase flow systems. *Journal of Heat Transfer*, 87(4):453–468, 11 1965. URL `http://dx.doi.org/10.1115/1.3689137`.

[14] J. P. Schlegel, P. Sawant, S. Paranjape, B. Ozar, T. Hibiki, and M. Ishii. Void fraction and flow regime in adiabatic upward two-phase flow in large diameter vertical pipes. *Nuclear Engineering and Design*, 239(12):2864–2874, 2009.

[15] Kataoka Isao and Ishii Mamoru. Drift flux model for large diameter pipe and new correlation for pool void fraction. *International Journal of Heat and Mass Transfer*, 30(9):1927 – 1939, 1987. ISSN 0017-9310. doi: http://dx.doi.org/10.1016/0017-9310(87)90251-1. URL `http://www.sciencedirect.com/science/article/pii/0017931087902511`.

[16] Xiuzhong Shen, Takashi Hibiki, and Hideo Nakamura. Developing structure of two-phase flow in a large diameter pipe at low liquid flow rate. *International Journal of Heat and Fluid Flow*, 34(0):70 – 84, 2012. ISSN 0142-727X. doi: http://dx.doi.org/10.1016/j.ijheatfluidflow.2012.02.004. URL `http://www.sciencedirect.com/science/article/pii/S0142727X12000240`.

[17] Yehuda Taitel, D. Bornea, and A. E. Dukler. Modelling flow pattern transitions for steady upward gas-liquid flow in vertical tubes. *AIChE Journal*, 26:345–354, 1980.

[18] Swanand M. Bhagwat and Afshin J. Ghajar. Similarities and differences in the flow patterns and void fraction in vertical upward and downward two phase flow. *Experimental Thermal and Fluid Science*, 39(0):213 – 227, 2012. ISSN 0894-1777. doi: http://dx.doi.org/10.1016/j.expthermflusci.2012.01.026. URL `http://www.sciencedirect.com/science/article/pii/S0894177712000374`.

[19] Pranav V. Godbole, Clement C. Tang, and Afshin J. Ghajar. Comparison of void fraction correlations for different flow patterns in upward vertical two-phase flow. *Heat Transfer Engineering*, 32(10):843–860, 2011. doi: 10.1080/01457632.2011.548285. URL `http://www.tandfonline.com/doi/abs/10.1080/01457632.2011.548285`.

[20] Ning Yang, Jianhua Chen, Wei Ge, and Jinghai Li. A conceptual model for analyzing the stability condition and regime transition in bubble columns. *Chemical Engineering Science*, 65(1):517 – 526, 2010. ISSN 0009-2509. doi: http://dx.doi.org/10.1016/j.ces.2009.06.014. URL `http://www.sciencedirect.com/science/article/pii/S0009250909003984`. 20th International Symposium in Chemical Reaction Engineering—Green Chemical Reaction Engineering for a Sustainable Future.

[21] Peter M. Wilkinson and Laurent L. v. Dierendonck. Pressure and gas density effects on bubble break-up and gas hold-up in bubble columns. *Chemical Engineering Science*, 45(8):2309 – 2315, 1990. ISSN 0009-2509. doi: http://dx.doi.org/10.1016/0009-2509(90)80110-Z. URL `http://www.sciencedirect.com/science/article/pii/000925099080110Z`.

[22] I. G. Reilly, D. S. Scott, T. J.W Debruijn, and D. Macintyre. The role of gas phase momentum in determining gas holdup and hydrodynamic flow regimes in bubble column operations. *The Canadian Journal of Chemical Engineering*, 72 (1):3–12, 1994. ISSN 1939-019X. doi: 10.1002/cjce.5450720102. URL `http://dx.doi.org/10.1002/cjce.5450720102`.

[23] P. Griffith and George A. Snyder. The bubbly-slug transition in a high velocity two phase flow the bubbly-slug transition in a high velocity two phase flow the bubbly-slug transition in a high velocity two phase flow. Technical report, Massachusetts Institute of Technology, Heat Transfer Laboratory, 1964.

[24] Joshua Schlegel, Takashi Hibiki, and Mamoru Ishii. Development of a comprehensive set of drift-flux constitutive models for pipes of various hydraulic diameters. *Progress in Nuclear Energy*, 52(7):666 – 677, 2010. ISSN 0149-1970. doi: http://dx.doi.org/10.1016/j.pnucene.2010.03.007. URL `http://www.sciencedirect.com/science/article/pii/S0149197010000600`.

[25] A.R. Hasan, C.S. Kabir, and M. Sayarpour. Simplified two-phase flow modeling in wellbores. *Journal of Petroleum Science and Engineering*, 72(1–2):42 – 49, 2010. ISSN 0920-4105. doi: http://dx.doi.org/10.1016/j.petrol.2010.02.007. URL `http://www.sciencedirect.com/science/article/pii/S0920410510000458`.

[26] A Hashemi, JH Kim, and JP Sursock. Effect of diameter and geometry on two-phase flow regimes and carry-over in a model pwr hot leg. In *Proceedings of 8th International Heat Transfer Conference, San Francisco, CA, USA*, pages 2443–2451, 1986.

[27] WH Hall, WP Prueter, TL Thome, and JR Wall. High-pressure steam/water void fraction profiles in a large-diameter, vertical pipe with non-developed entrance flow. In *Thermal hydraulics of nuclear steam generators/heat exchangers: presented at the Winter Annual Meeting of the American Society of Mechanical Engineers, Chicago, Illinois, November 27-December 2, 1988*, volume 102, page 53. The Society, 1988.

[28] T.R. Smith, J.P. Schlegel, T. Hibiki, and M. Ishii. Two-phase flow structure in large diameter pipes. *International Journal of Heat and Fluid Flow*, 33(1):156 – 167, 2012. ISSN 0142-727X. doi: http://dx.doi.org/10.1016/

j.ijheatfluidflow.2011.10.008. URL http://www.sciencedirect.com/science/article/pii/S0142727X11001469.

[29] Juei-Tsuen Hsu, Mamoru Ishii, and Takashi Hibiki. Experimental study on two-phase natural circulation and flow termination in a loop. *Nuclear Engineering and Design*, 186(3):395 – 409, 1998. ISSN 0029-5493. doi: http://dx.doi.org/10.1016/S0029-5493(98)00285-4. URL http://www.sciencedirect.com/science/article/pii/S0029549398002854.

[30] Y. Inoue. *Measurement of Interfacial Area Concentration of Gas–Liquid Two Phase Flow in a Large Diameter Pipe*. PhD thesis, MS Thesis. Graduate School of Energy Science, Kyoto University, 2001.

[31] Kimitoshi Yoneda, Akira Yasuo, and Tomio Okawa. Flow structure and bubble characteristics of steam–water two-phase flow in a large-diameter pipe. *Nuclear Engineering and Design*, 217(3):267 – 281, 2002. ISSN 0029-5493. doi: http://dx.doi.org/10.1016/S0029-5493(02)00157-7. URL http://www.sciencedirect.com/science/article/pii/S0029549302001577.

[32] Branko Stankovic. *An experimental study on the local void fraction measurements in large diameter vertical pipes using optical fiber probes*. PhD thesis, University of Hamilton, Ontario, 1997.

[33] M. Elena Díaz, Francisco J. Montes, and Miguel A. Galán. Influence of the lift force closures on the numerical simulation of bubble plumes in a rectangular bubble column. *Chemical Engineering Science*, 64(5):930 – 944, 2009. ISSN 0009-2509. doi: http://dx.doi.org/10.1016/j.ces.2008.10.055. URL http://www.sciencedirect.com/science/article/pii/S000925090800609X.

[34] Allison F. Studley. *Numerical Modeling of Air-Water Flows in Bubble Columns and Airlift Reactors*. PhD thesis, Virginia Polytechnic Institute, 2010.

[35] M. Simonnet, C. Gentric, E. Olmos, and N. Midoux. Cfd simulation of the flow field in a bubble column reactor: Importance of the drag force formulation to describe regime transitions. *Chemical Engineering and Processing: Process Intensification*, 47(9–10):1726 – 1737, 2008. ISSN 0255-2701. doi: http://dx.doi.org/10.1016/j.cep.2007.08.015. URL http://www.sciencedirect.com/science/article/pii/S025527010700308X.